AMERICAN SOCIETY FOR MICROBIOLOGY | Journal of Bacteriology®

RESEARCH ARTICLE

Bacterial Homologs of Progestin and AdipoQ Receptors (PAQRs) Affect Membrane Energetics Homeostasis but Not Fluidity

Maddison V. Melchionna,[a] Jessica M. Gullett,[a]* Emmanuelle Bouveret,[b] Him K. Shrestha,[c,d] Paul E. Abraham,[c] Robert L. Hettich,[c] Gladys Alexandre[a]

[a]Department of Biochemistry and Cellular and Molecular Biology, University of Tennessee, Knoxville, Tennessee, USA
[b]Institut Pasteur, UMR 2001 CNRS, Paris, France
[c]Bioscience Division, Oak Ridge National Laboratory, Oak Ridge, Tennessee, USA
[d]Genome Science and Technology, University of Tennessee, Knoxville, Tennessee, USA

ABSTRACT Membrane potential homeostasis is essential for cell survival. Defects in membrane potential lead to pleiotropic phenotypes, consistent with the central role of membrane energetics in cell physiology. Homologs of the progestin and AdipoQ receptors (PAQRs) are conserved in multiple phyla of *Bacteria* and *Eukarya*. In eukaryotes, PAQRs are proposed to modulate membrane fluidity and fatty acid (FA) metabolism. The role of bacterial homologs has not been elucidated. Here, we use *Escherichia coli* and *Bacillus subtilis* to show that bacterial PAQR homologs, which we name "TrhA," have a role in membrane energetics homeostasis. Using transcriptional fusions, we show that *E. coli* TrhA (encoded by *yqfA*) is part of the unsaturated fatty acid biosynthesis regulon. Fatty acid analyses and physiological assays show that a lack of TrhA in both *E. coli* and *B. subtilis* (encoded by *yplQ*) provokes subtle but consistent changes in membrane fatty acid profiles that do not translate to control of membrane fluidity. Instead, membrane proteomics in *E. coli* suggested a disrupted energy metabolism and dysregulated membrane energetics in the mutant, though it grew similarly to its parent. These changes translated into a disturbed membrane potential in the mutant relative to its parent under various growth conditions. Similar dysregulation of membrane energetics was observed in a different *E. coli* strain and in the distantly related *B. subtilis*. Together, our findings are consistent with a role for TrhA in membrane energetics homeostasis, through a mechanism that remains to be elucidated.

IMPORTANCE Eukaryotic homologs of the progestin and AdipoQ receptor family (PAQR) have been shown to regulate membrane fluidity by affecting, through unknown mechanisms, unsaturated fatty acid (FA) metabolism. The bacterial homologs studied here mediate small and consistent changes in unsaturated FA metabolism that do not seem to impact membrane fluidity but, rather, alter membrane energetics homeostasis. Together, the findings here suggest that bacterial and eukaryotic PAQRs share functions in maintaining membrane homeostasis (fluidity in eukaryotes and energetics for bacteria with TrhA homologs).

KEYWORDS bacteria, fatty acid biosynthesis, membrane energetics, membrane potential, PAQRs

Biological membranes are semipermeable barriers composed of proteins, which impart their biological functions, and lipids, which modulate biophysical properties (1). Maintaining membrane homeostasis is essential for cell survival. The lipid composition of membranes varies with cell type, organelle, and environmental conditions (2, 3). Membrane lipid composition, in particular its fatty acid moiety, imposes constraints on the physicochemical properties of the bilayer and controls membrane protein insertion, folding, and function (3, 4). Defects in membrane lipid homeostasis are associated

Editor Michael Y. Galperin, NCBI, NLM, National Institutes of Health

Copyright © 2022 Melchionna et al. This is an open-access article distributed under the terms of the Creative Commons Attribution 4.0 International license.

Address correspondence to Gladys Alexandre, galexan2@utk.edu.

*Present address: Jessica M. Gullett, Department of Immunology, St. Jude Children's Research Hospital, Memphis, Tennessee, USA.

The authors declare no conflict of interest.

Received 19 November 2021
Accepted 28 January 2022
Published 14 March 2022

with multiple cellular stresses and metabolic changes (5, 6). Organisms regulate the lipid composition of membranes using diverse mechanisms that target phospholipids and fatty acids (1, 7–9) to adjust membrane function to changes in the biophysical properties of the membrane bilayer (10).

The physicochemical properties of membranes are also essential for the maintenance of concentration and electrical gradients that comprise the membrane potential ($\Delta\psi$) and power physiological work (11). The establishment of gradients across membranes directly results from their differential permeability to ions and charged molecules. Changes in $\Delta\psi$ have been best described in excitable cells such as neurons (12). However, recent experimental evidence indicates that most "nonexcitable" animal cells (12), as well as bacteria (13–15), have a dynamic $\Delta\psi$. In bacteria, dynamic $\Delta\psi$ generates electrical signals that regulate intra- and interspecies communications in biofilms and serve as signals for mechanosensing (14, 16, 17).

Like eukaryotes, the bacterial $\Delta\psi$ is established through the activity of ion channels and transporters of monovalent/divalent cations and charged organic molecules (18–21). The bacterial transmembrane potential powers diverse physiological functions, including ATP synthesis, motility, pH homeostasis, electrical communication, resistance to antibiotics, cellular growth and division, and molecular transport (11). The transmembrane proton gradient (ΔpH) and the transmembrane electrical potential ($\Delta\Psi$) comprise the proton motive force (PMF), which plays an essential role in bacterial physiology (11). Homeostasis of the PMF is maintained by altering either the ΔpH or $\Delta\Psi$; if the $\Delta\Psi$ is collapsed, bacteria compensate for this loss by increasing ΔpH (22). In both eukaryotes and bacteria, voltage-gated ion channels modulate their transport activity in response to changes in the electrical gradient across the membrane and are major regulators of the transmembrane electrochemical gradients (18, 23).

Here, we show that a membrane protein of unknown function in two *Escherichia coli* (encoded by *yqfA*) strains and the distantly related *Bacillus subtilis* (encoded by *yplQ*) modulates the ability of cells to maintain optimal (i.e., wild-type [WT]-like) membrane energetics, as reported by measuring alterations in dye fluorescence reflecting the changes in the membrane potential, which we refer to as membrane energetics homeostasis. We named this protein TrhA for "transmembrane homeostasis" protein A. TrhA is not related to voltage-gated channels or to transporters of ions, metals, or organic molecules but is related to the progestin and AdipoQ receptor (PAQR) family of proteins (24). PAQRs are conserved across multiple phyla of *Bacteria* and *Eukarya* (24). In eukaryotes, the PAQR superfamily includes three classes of membrane receptors (24). Class I PAQRs are related to the human adiponectin receptors (AdipoRs) and respond to adiponectin (25, 26). The PAQR homologs in humans and *Caenorhabditis elegans* function to maintain membrane fluidity and membrane fatty acid composition in response to conditions which rigidify the membrane (27–30). Class II PAQRs respond to progesterone (31–33). Class III PAQRs are phylogenetically closely related to bacterial TrhA/PAQR homologs (24). These proteins are proposed to function as hemolysin-III proteins because expression of recombinant bacterial homologs induces cytolysis of eukaryotic cells (34, 35). Results reported here implicate bacterial TrhA homologs in the maintenance of membrane energetics homeostasis, with membrane potential measurement as a reliable read-out.

RESULTS

The gene coding for TrhA is part of the *E. coli* FabR regulon. TrhA in *E. coli* ($TrhA_{EC}$) is encoded by *yqfA*. In *E. coli*, several studies suggested that FabR, the repressor of unsaturated fatty acid synthesis genes, binds to the promoter of *yqfA* ($trhA_{EC}$), in addition to the promoters of *fabA* and *fabB* (36, 37). The position of the FabR binding site relative to the transcription start site of $trhA_{EC}$ (38) is consistent with FabR acting as a repressor (Fig. 1A). However, the regulation of $trhA_{EC}$ by FabR *in vivo* suggested by global transcriptome analyses (39) was not confirmed in a subsequent study (36), maybe because the experiment in this later study was performed in the BW25113

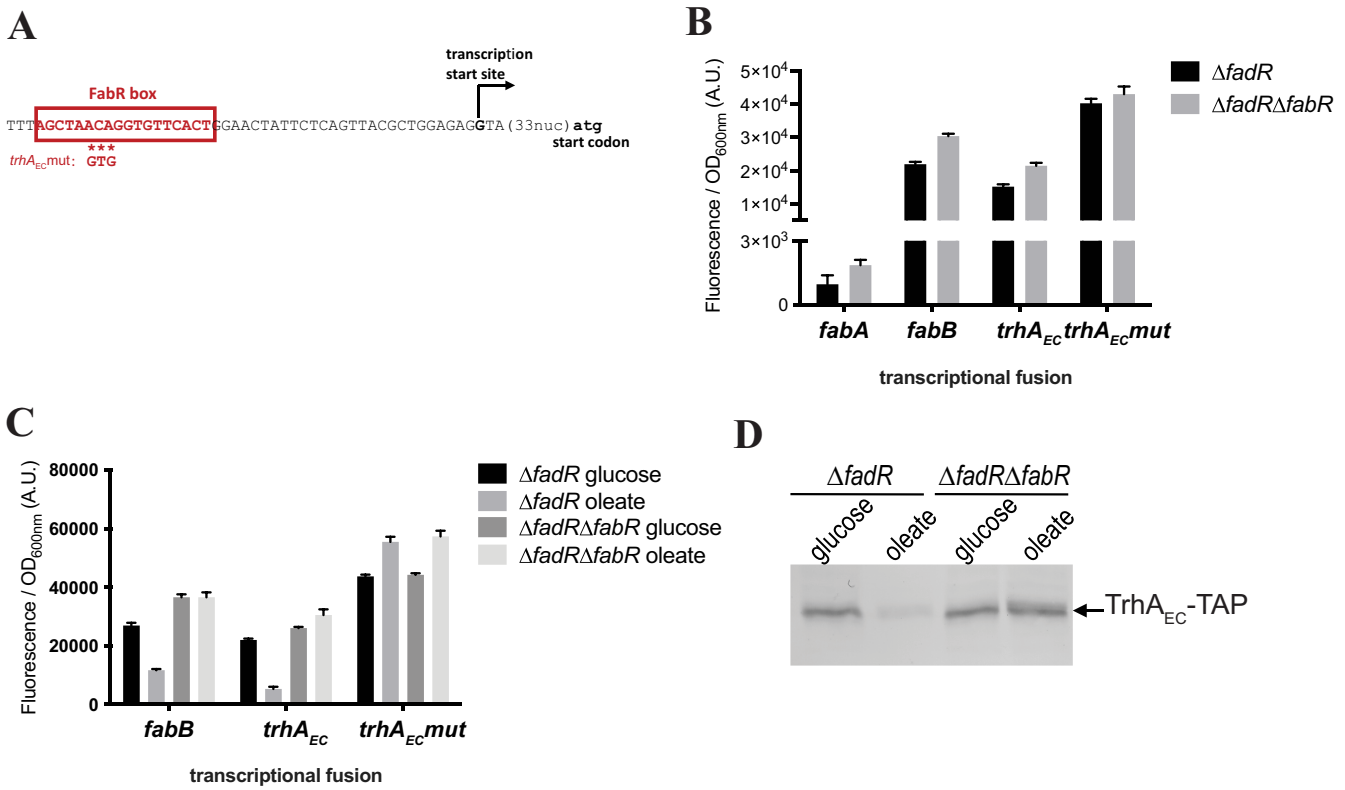

FIG 1 The gene coding for TrhA in *E. coli* is coregulated with genes of unsaturated fatty acid synthesis. (A) Sequence of the $trhA_{EC}$ promoter. The transcription start site corresponds to the one identified in reference 38. The FabR box was identified in reference 36. The mutations introduced in the FabR box are indicated below the sequence. (B) Strains Δ*fadR* and Δ*fadR*Δ*fabR* were transformed by the plasmids containing the indicated transcriptional fusions. Relative fluorescence intensities were measured after overnight growth at 30°C in LB supplemented with kanamycin (see Materials and Methods). (C) Strains Δ*fadR* and Δ*fadR*Δ*fabR* were transformed by the plasmids containing the indicated transcriptional fusions. Relative fluorescence intensities were measured after overnight growth at 30°C in M9 minimal medium with 0.2% glucose or 0.2% oleate as the carbon source. (D) Strains Δ*fadR* and Δ*fadR*Δ*fabR* were transformed by the pUA-trhA-TAP plasmid. Cultures were performed at 37°C in M9 minimal medium with 0.2% glucose or 0.2% oleate as the carbon source. Total lysates were then analyzed by Western blotting using anti-TAP antibodies.

strain reported to contain a mutation in *fabR* (39). We used transcriptional fusions with green fluorescent protein (GFP) (40) to compare the expression of $trhA_{EC}$ in the presence or absence of FabR in a Δ*fadR* genetic background to isolate the FabR regulation effects as previously described (36). The expression of $trhA_{EC}$ was upregulated in the Δ*fabR* strain as efficiently as for *fabB* (Fig. 1B). Mutations of three nucleotides in the FabR binding box in the promoter of $trhA_{EC}$ ($trhA_{EC}$ mut) increased $trhA_{EC}$ expression, while the $trhA_{EC}$ mut expression no longer increased in the Δ*fabR* mutant (Fig. 1B). Oleate, which promotes FabR repression, strongly repressed $trhA_{EC}$ expression, but not the $trhA_{EC}$ mut expression (Fig. 1C). This effect, dependent on the presence of FabR, was also observed by monitoring levels of $TrhA_{EC}$-TAP protein (Fig. 1D). Taken together, these data confirm that $trhA_{EC}$ is regulated by FabR, suggesting that it may influence fatty acid membrane composition.

The Δ$trhA_{EC}$ mutant derivative of *E. coli* has subtle changes in its fatty acid composition compared to *E. coli* WT. The eukaryotic PAQRs characterized to date are implicated in FA metabolism or modification of phospholipids to adjust membrane fluidity (27–29, 41–45). Thus, we analyzed the FA composition of *E. coli* membranes from WT and strains lacking the TrhA homolog (Δ$trhA_{EC}$) grown at physiological (37°C) and low (16°C) temperatures to challenge cells with membrane rigidity stress. When grown at 37°C, the Δ$trhA_{EC}$ strain produced fewer long, unsaturated C18:1w7c FAs and fewer C13:0 and C13:0 hydroxy FAs than the WT (Fig. 2A). It also produced more saturated C14:0 FAs and C17:0 cyclopropanes than the WT (Fig. 2A). At 16°C, the Δ$trhA_{EC}$ strain only increased its abundance of C17:0 cyclopropanes compared to the WT (Fig. 2B). Cells lacking $TrhA_{EC}$ thus have subtle changes in membrane FA composition compared

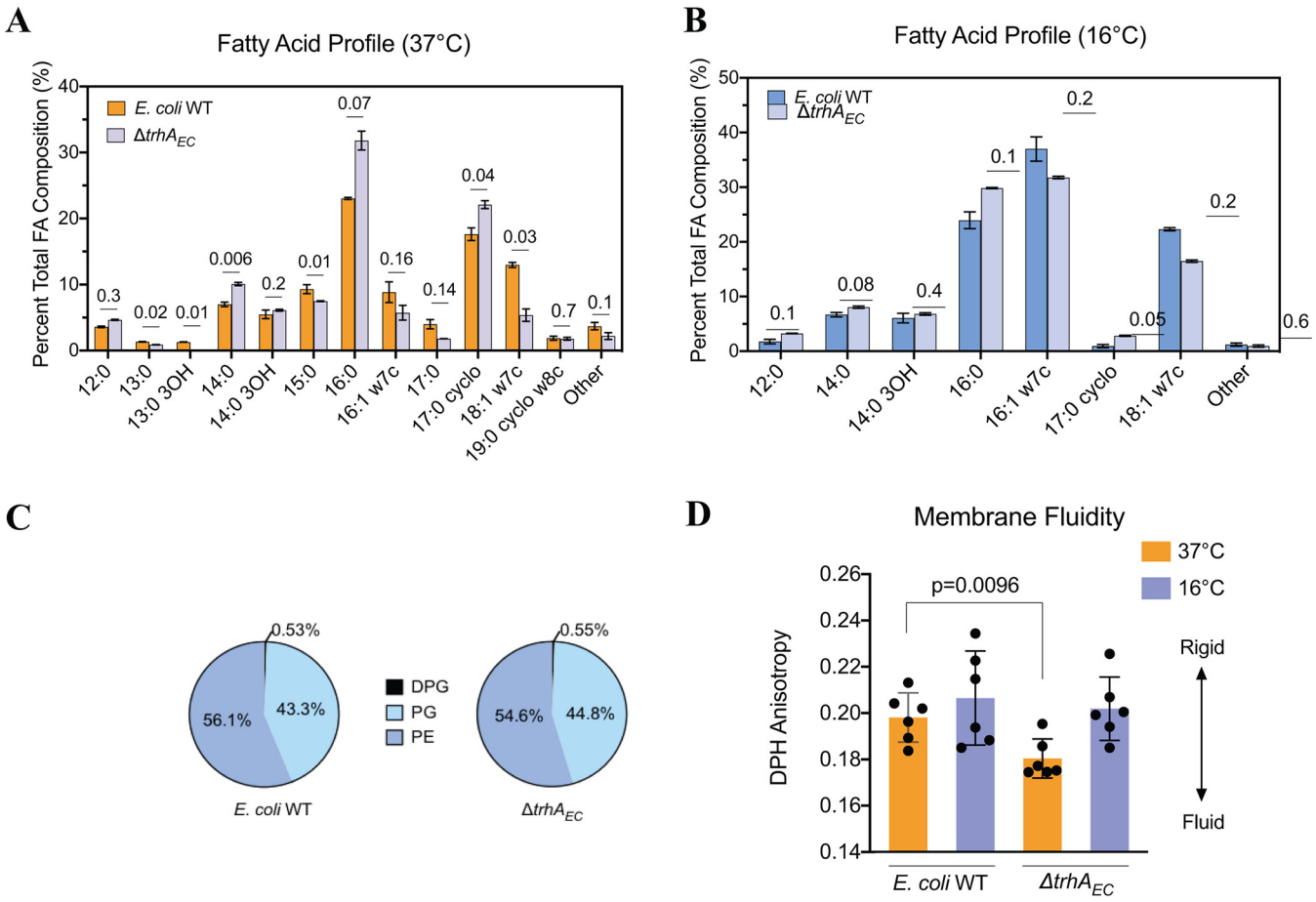

FIG 2 Control of membrane fluidity is not the primary role of $TrhA_{EC}$. (A) Total fatty acid composition of *E. coli* WT and the Δ*trhA*$_{EC}$ strain grown at 37°C. (B) Total fatty acid composition of *E. coli* WT and the Δ*trhA*$_{EC}$ strain grown at 16°C. Error bars represent the standard deviation of two biological and two technical replicates. *P* values are listed above each set of bars. (C) Phospholipid headgroup analysis of *E. coli* WT and the Δ*trhA*$_{EC}$ strain. The percent compositions of phosphatidylethanolamine (PE) lipids, diphosphatidylglycerol (PG) lipids, and diphosphatidylglycerol (DPG)/cardiolipin lipids are the averages from three biological replicates. (D) Membrane fluidity of *E. coli* WT and the Δ*trhA*$_{EC}$ mutant. The membrane fluidity of whole cells was measured using DPH anisotropy, where greater values in anisotropy indicate a more rigid membrane. The data represent six biological replicates, where each point is the average of three technical replicates. Error bars represent the standard deviation.

to the WT, but there were no significant differences in the proportions of phospholipid headgroups produced by either strain (Fig. 2C).

The Δ*trhA*$_{EC}$ mutant made adjustments to its FA profile similar to those of the WT (see Fig. S1A in the supplemental material). Both strains decreased their production of short, saturated FA and C17:0 cyclopropanes at 16°C compared to 37°C, and both increased production of long, unsaturated C16:1 w7c at 16°C (Fig. S1B). These findings indicate that $TrhA_{EC}$ has small effects on FA composition, but it is not specifically implicated in a temperature-mediated membrane rigidity stress response.

Membrane fluidity control is not the primary function of $TrhA_{EC}$. Next, we used 1,6-diphenyl 1,3,5-hexatriene (DPH) to compare the membrane fluidity of *E. coli* WT and the Δ*trhA*$_{EC}$ strain grown at 37°C and 16°C. The fluorescence anisotropy of DPH increases in ordered membranes and decreases in fluid membranes (46). For WT, the net membrane fluidity remained constant from 37°C to 16°C (Fig. 2D), consistent with *E. coli* maintaining fluidity across a range of growth temperatures (47). The Δ*trhA*$_{EC}$ mutant membrane was more fluid at 37°C than at 16°C and was comparable to that of *E. coli* WT at 16°C (Fig. 2D). These data are consistent with the subtle effects of a Δ*trhA*$_{EC}$ mutation on membrane FA composition at this temperature (Fig. 2B) and highlight an incongruency between the membrane fluidity and FA compositions of the Δ*trhA*$_{EC}$ strain at 37°C. The Δ*trhA*$_{EC}$ strain's membrane is expected to be more rigid than that of the WT at 37°C, given the membrane FA profiles of the mutant (i.e., fewer long,

unsaturated FAs and more saturated FAs than *E. coli* WT), but we found fluidity was increased (Fig. 2D). The primary function of $TrhA_{EC}$ is thus unlikely to be membrane fluidity regulation.

Membrane proteomics support a negligible effect on membrane fluidity. Next, we compared the membrane proteomes of *E. coli* WT and the Δ*trhA*$_{EC}$ strain, grown at 37°C and 16°C to identify membrane-specific function(s) associated with $TrhA_{EC}$. The analysis captured soluble proteins that are overly abundant and/or which interact at the membrane. At both temperatures, Δ*trhA*$_{EC}$ had a membrane proteome with pleiotropic changes compared to the WT, suggesting a major role for $TrhA_{EC}$ in cell physiology (Fig. 3). A total of 301 proteins were differentially abundant in the Δ*trhA*$_{EC}$ strain compared to *E. coli* WT and belonged to distinct functional groups based on Gene Ontology (GO-term) categories (Fig. 3 and Tables S1 and S2) (48).

Analysis of the Δ*trhA*$_{EC}$ mutant membrane proteome did not provide evidence for a prominent role in membrane fluidity. Compared to *E. coli* WT, the Δ*trhA*$_{EC}$ mutant produced lower abundances of FabA and FabF at 37°C (Table S1A) and slightly higher abundances of FabG at 37°C and FabH at 16°C (Table S1B). TesB, which is implicated in FA turnover, was more abundant in the Δ*trhA*$_{EC}$ mutant at 37°C compared to *E. coli* WT (Table S1B). These changes do not correlate with the net membrane fluidity increase of the mutant at 37°C; the increase in FA elongation enzyme FabG and decrease in unsaturated FA synthesis protein FabA are expected to result in a more rigid membrane for the mutant. Altered abundances of these proteins in the Δ*trhA*$_{EC}$ mutant were not common across the two temperatures, suggesting that other confounding factors affect FA composition and membrane fluidity in the mutant. No other proteins with known functions in FA metabolism that would suggest a role in membrane fluidity were differentially expressed. Outer membrane proteins (OMPs) and lipoproteins decreased in abundance in the Δ*trhA*$_{EC}$ proteome compared to the WT (Fig. 3C and D and Table S1A). Relative to the WT, proteins involved in cell surface structure and membrane remodeling increased and decreased in abundance, respectively, in the Δ*trhA*$_{EC}$ strain (Fig. 3C and D and Table S1A and B). These findings are consistent with $TrhA_{EC}$ exerting pleiotropic effects on homeostasis of the membrane.

***E. coli* strains lacking *trhA*$_{EC}$ are impaired in motility and membrane energetics.** The most profound change in the Δ*trhA*$_{EC}$ membrane proteome relative to *E. coli* WT was the reduction in abundance of flagellar and chemotaxis proteins (Fig. 3B and Table S1B). Compared to *E. coli* WT we also observed by light microscopy that the Δ*trhA*$_{EC}$ mutant cells either did not swim or swam slowly in liquid media, suggesting that some flagella are present, and it did not chemotax in semisoft agar plates, consistent with impaired motility (Fig. 4A).

Membrane proteomics indicated that transporters, proton symporters, and antiporter proteins, most of which transport positively charged amino acids, divalent cations, and positively charged metals, were lower in abundance in the Δ*trhA*$_{EC}$ strain than in the WT (Fig. 3B to D and Table S1A). For example, substrate(s) denoted FeoB (Fe^{2+}), HisQ (lysine, arginine, ornithine, and histidine), NikC (Ni^{2+}), ZntA (Zn^{2+}/Cd^{2+}/Pb^{2+}), and ZntB (Zn^{2+}:H^{+}) were reduced in abundance in the Δ*trhA*$_{EC}$ mutant relative to *E. coli* WT (Tables S1B and S2). Proteins involved in aerobic and anaerobic respiratory redox chains which pump protons, including dehydrogenases SdhD, NuoBJ, and HybA, and terminal reductases and oxidases NarGH, FrdD, and CyoA were less abundant in the mutant than in the WT (Fig. 3C and D and Table S1A). At 37°C, the mutant also reduced the abundance of three components of the ATP synthase complex (AtpDHG) (Table S1A). Consistent with these changes, the mutant produces less ATP than the WT (Fig. 4B). Proteomics thus suggest that the abundance of proteins that regulate or utilize gradients of charged molecules across the membrane, including protons, charged amino acids, metals such as iron, zinc, nickel (Table S1A), and ATP synthesis, are perturbed by the lack of TrhA. These changes are expected to affect membrane energetics.

$TrhA_{EC}$ in *E. coli* is required for optimal (WT-like) membrane potential. To test the role of TrhA in membrane energetics, we used two fluorescent, hydrophobic, cationic reporters, $DiOC_2(3)$ and ThT, to compare the membrane potential ($\Delta\psi$) of *E. coli*

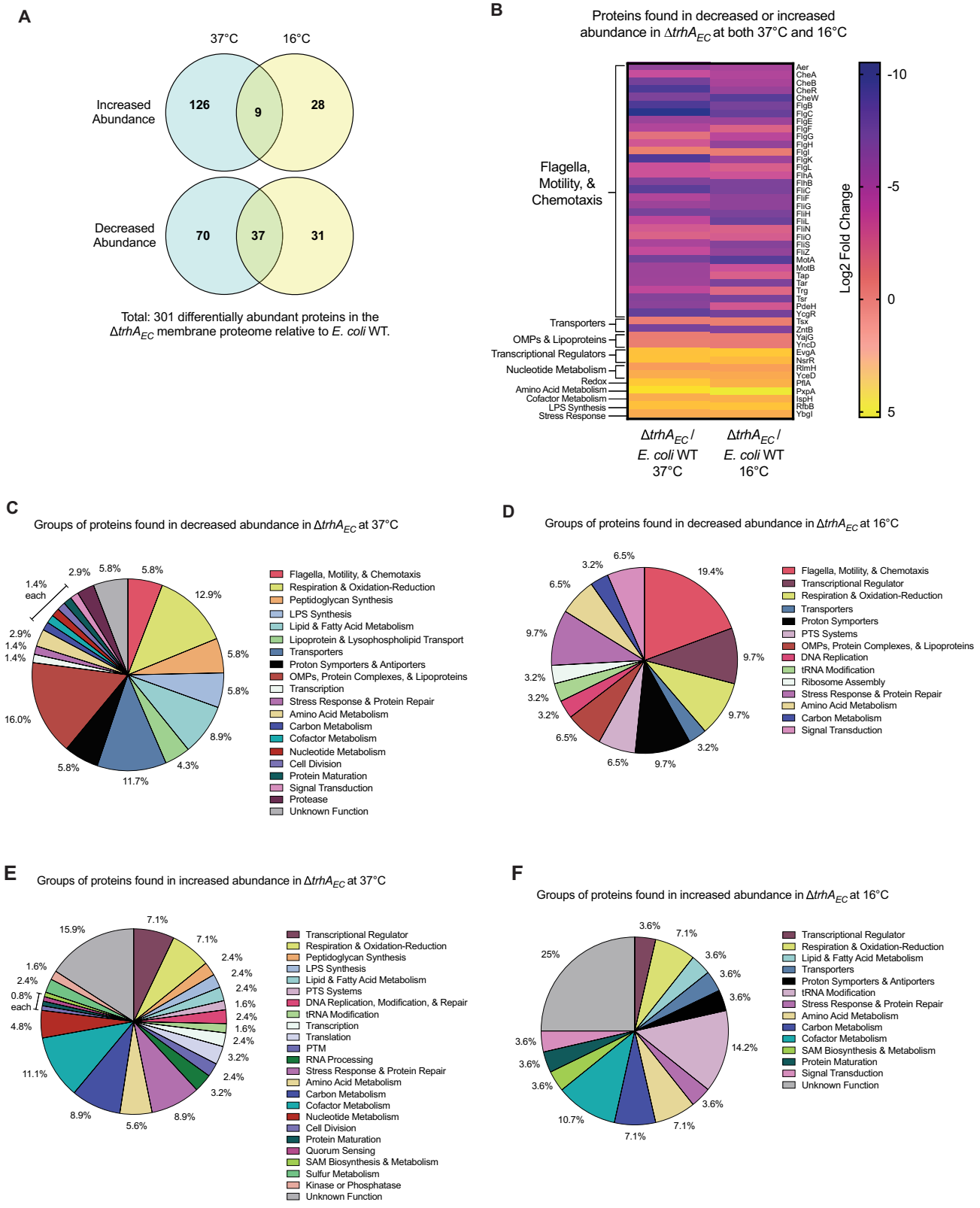

FIG 3 Membrane proteome of the Δ*trhA*$_{EC}$ mutant reveals large changes in protein abundance, cellular physiology, and metabolism. (A) Venn diagram representing numbers of the differentially abundant proteins in the membrane proteome of Δ*trhA*$_{EC}$ relative to *E. coli* WT. (B) Heat map of proteins that are found in decreased or increased abundance at both 37°C and 16°C in the membrane proteome of Δ*trhA*$_{EC}$ relative to *E. coli* WT. The average $\log_2$ fold change of six biological replicates is represented. (C and D) Representation of proteins that are found in decreased abundance in the membrane proteome of ΔtrhA$_{EC}$ relative to WT *E. coli* at (C) 37°C and (D) 16°C. Proteins are functionally classified into GO-terms. (E and F) Representation of proteins that are found in increased abundance in the membrane proteome of Δ*trhA*$_{EC}$ relative to WT *E. coli* at (E) 37°C and (F) 16°C.

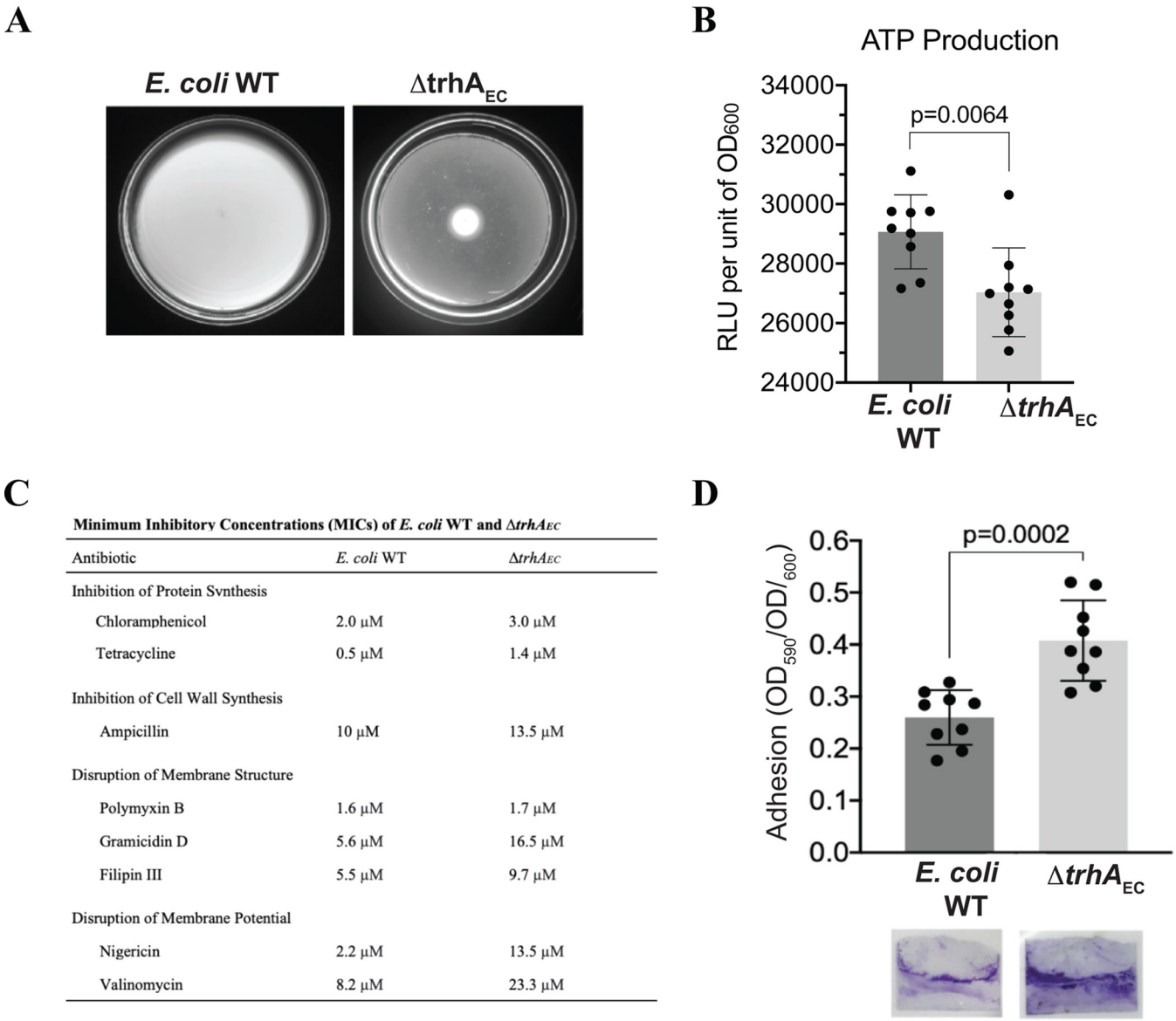

Minimum Inhibitory Concentrations (MICs) of *E. coli* WT and Δ*trhA*$_{EC}$

Antibiotic	*E. coli* WT	Δ*trhA*$_{EC}$
Inhibition of Protein Svnthesis		
Chloramphenicol	2.0 μM	3.0 μM
Tetracycline	0.5 μM	1.4 μM
Inhibition of Cell Wall Synthesis		
Ampicillin	10 μM	13.5 μM
Disruption of Membrane Structure		
Polymyxin B	1.6 μM	1.7 μM
Gramicidin D	5.6 μM	16.5 μM
Filipin III	5.5 μM	9.7 μM
Disruption of Membrane Potential		
Nigericin	2.2 μM	13.5 μM
Valinomycin	8.2 μM	23.3 μM

FIG 4 Physiology of the Δ*trhA*$_{EC}$ mutant supports defective membrane energetics. (A) *E. coli* WT and Δ*trhA*$_{EC}$ mutant cells were plated on the center of a soft agar (0.3%) plate. The plates were imaged after 18 h of incubation at 28°C. (B) The total ATP production of stationary-phase *E. coli* WT and Δ*trhA*$_{EC}$ mutant cells was measured as luminescence relative light units (RLU). Data represent the ATP content from three biological replicates with three technical replicates. Error bars represent the standard deviation. (C) MICs of *E. coli* WT and the Δ*trhA*$_{EC}$ strain for different antibiotics. MIC values represent the average concentration of antibiotic (in μM) that observably inhibited the growth of three to five biological replicates with three technical replicates each. (D) Biofilm production of *E. coli* WT and the Δ*trhA*$_{EC}$ mutant. Cultures were grown overnight in 12-well plates containing a sterile microscope slide. Biofilms that adhered to the air-liquid interface of a coverslip were stained with crystal violet and quantified at OD$_{590}$. The OD$_{590}$ was normalized to cell growth as OD$_{600}$. Points represent quantifications of biofilm produced from three biological replicates with three technical replicates. Error bars represent the standard deviation.

WT and the Δ*trhA*$_{EC}$ strain. DiOC$_2$(3) and ThT fluoresce once accumulated within polarized cells (49), but their fluorescence decreases upon membrane depolarization (49). Depolarization using carbonyl cyanide m-chlorophenyl hydrazone (CCCP) caused DiOC$_2$(3) and ThT fluorescence to decrease relative to the dimethyl sulfoxide (DMSO) controls in both WT and Δ*trhA*$_{EC}$ strains (Fig. 5A and B). However, the resting membrane potential ($\Delta\psi$) of the Δ*trhA*$_{EC}$ mutant was significantly depolarized compared to that of the WT (Fig. 5A and B). While similar dyes have been used by others (e.g., 13–16), we note that fluorescent reporters for membrane potential are active within specific ranges (50). We expect a technical limitation in the ability to capture the absolute dynamic range of membrane potential.

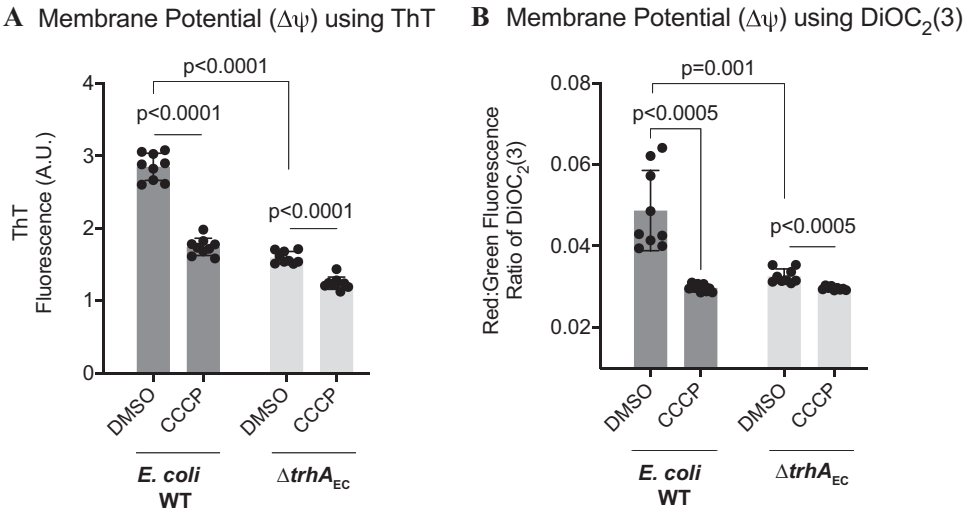

FIG 5 Cells lacking $TrhA_{EC}$ have a depolarized membrane. (A and B) The membrane potential of *E. coli* WT and the Δ*trhA*$_{EC}$ strain was measured using (A) ThT and (B) DiOC2(3) fluorescent reporters. DMSO treatments represent the resting membrane potential of cells. The membrane potential of each strain was collapsed when treated with CCCP, as indicated by decreased reporter fluorescence. The data represent fluorescence from three biological replicates with three technical replicates. Error bars represent the standard deviation.

Expressing parental *trhA*$_{EC}$ from a low-copy-number plasmid (51) in the Δ*trhA*$_{EC}$ strain (Δ*trhA*$_{EC}$ [pRH005 *trhA*$_{EC}$]) restored the mutant $\Delta\psi$ to near-WT levels (Fig. 6A). This complemented Δ*trhA*$_{EC}$ mutant strain had a higher resting $\Delta\psi$ than the Δ*trhA*$_{EC}$ (pRH005) mutant that was not significantly different from that of the *E. coli* WT (pRH005) (Fig. 6A). The motility defect of the Δ*trhA*$_{EC}$ mutant was also partially complemented in this strain (Fig. 6B and Fig. S2A). Our attempts to perform functional complementation using inducers or different-copy-number plasmids (pTrc99a, pBAD33) failed to produce complementation (Fig. S2B and C). Poor transport of the inducers could be implicated here, given the altered membrane proteome and membrane energetics of Δ*trhA*$_{EC}$. The inability to transport these inducers could contribute to the minimal expression of $TrhA_{EC}$ from any plasmid or promoter. An alternative or additional

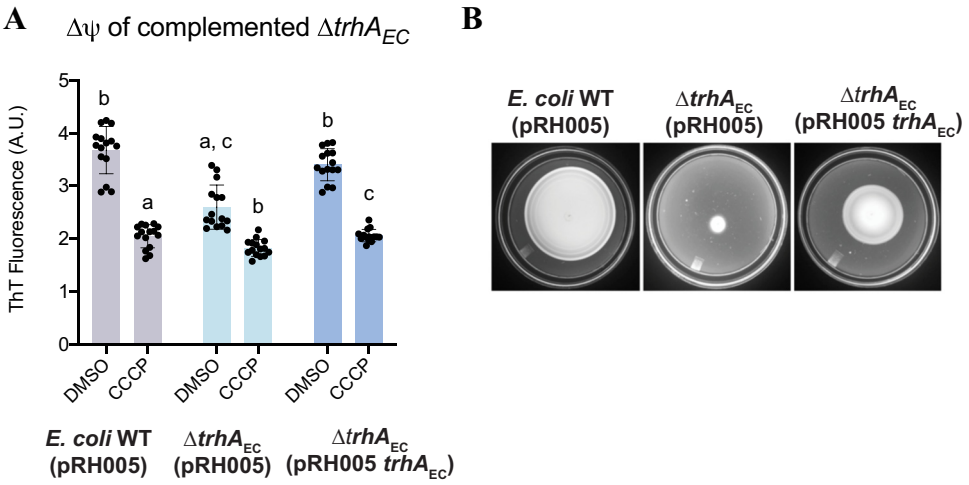

FIG 6 Functional complementation of the Δ*trhA*$_{EC}$ strain by expressing WT *trhA*$_{EC}$ using the pRH005 plasmid. (A) Membrane potentials of *E. coli* WT (pRH005), Δ*trhA*$_{EC}$ (pRH005), and Δ*trhA*$_{EC}$ (pRH005) were measured using ThT. Data represent fluorescence from five biological replicates with three technical replicates. Error bars represent the standard deviation. a, significantly different from *E. coli* WT (pRH005) DMSO ($P < 0.05$); b, significantly different from Δ*trhA*$_{EC}$ (pRH005) DMSO ($P < 0.05$); c, significantly different from Δ*trhA*$_{EC}$ (pRH005 *trhA*$_{EC}$) DMSO ($P < 0.05$). (B) *E. coli* WT (pRH005), Δ*trhA*$_{EC}$ (pRH005), and Δ*trhA*$_{EC}$ (pRH005 *trhA*$_{EC}$) cells were plated on the center of a soft agar (0.3%) plate. Plates were imaged after 18 h of incubation at 28°C.

possibility is that the cellular stoichiometry of $TrhA_{EC}$ could also be a determining factor in its yet unknown function. Consistent with this notion, expressing pRH005 with $trhA_{EC}$ in the parental *E. coli* WT strain, thereby increasing the abundance of $TrhA_{EC}$, produces a dominant negative phenotype (Fig. S3A to C).

The effect of $TrhA_{EC}$ on the mutant membrane potential compared to its parent but the lack of a measurable growth defect (Table S3) prompted us to analyze the sequenced genomes of the *E. coli* WT and Δ$trhA_{EC}$ strains. None of the few genotypic changes detected in the genome of the Δ$trhA_{EC}$ strain relative to the *E. coli* WT strain explained the effect of $TrhA_{EC}$ on the membrane proteomes or energetics (Table S4). These mutations are either commonly found in laboratory strains of *E. coli* (*ins*B-5 and *ins*A-5) (52), are in a pseudogene (*stfE*), or have a predicted function in DNA recombination (*rmuC*). The only exception is a mutation in *pgk*, which encodes the glycolytic enzyme phosphoglycerate kinase (52). However, complementation of the Δ$trhA_{EC}$ strain using WT *pgk* in pRH005 did not restore motility to the mutant (Fig. S4A) or its membrane potential compared to the WT (Fig. S4B). These results are in agreement with functional (albeit partial) complementation of the *trhA* mutation and the dominant negative phenotype upon overexpression of *trhA* described above.

Modified metabolism and multiple stresses are associated with dysregulated membrane energetics. Consistent with altered membrane energetics, metabolic changes were evidenced in the mutant proteome relative to the WT (Fig. 3B to F and Tables S1 and S2). The Δ$trhA_{EC}$ mutant increased abundances of proteins which synthesize cofactors (cofactor annotated)—CoaA (coenzyme A), PanC (pantothenate), IspAE (isoprenoids), LipA (fatty acid anion lipoate), UbiC (ubiquinone), NadE (NAD^+), HemHL (heme), MoeA (molybdenum), RibC (riboflavin), ThiL (thiamine), and EntC (enterobactin) (Fig. 3B, E, and F and Table S1B). Enzymes involved in glycolysis, the glyoxylate shunt pathway, and the production of glyoxylate, increased in the mutant relative to the WT. Changes in abundance of proteins were implicated in amino acid and nucleotide metabolism (Fig. 3B, E, and F and Tables S1B and S2). DNA replication and modification (Fig. 3C to F and Tables S1B and S2), transcription, and translation (Fig. 3E and F and Tables S1B and S2) were affected in the mutant relative to the wild type. These changes suggest that the mutant's metabolism is dedicated to conservation of carbon, replenishment of metabolic intermediates, turnover pool of cofactors, and remodeling of information transfer processes.

Stress resistance responses were increased in the mutant compared to *E. coli* WT. The abundance of proteins with function in DNA damage repair and iron-sulfur cluster repair as well as glutaredoxin systems which help maintain oxidative states of small redox-sensitive thiol sensor proteins (53) increased in the Δ$trhA_{EC}$ mutant proteome (Fig. 3E and F and Table S1B), suggestive of upregulation of oxidative stress pathways. Reduction in the abundance of Cyo and Nuo proton-pumping complexes in the Δ$trhA_{EC}$ mutant compared to the WT could suggest mild alkaline stress (Fig. 3B to D and Table S1A), as *E. coli* reduces these complexes when grown at alkaline pH (54). The abundance of several transcriptional regulators important for acid and osmotic stress responses increased in the Δ$trhA_{EC}$ strain compared to *E. coli* WT (Fig. 3E and F and Table S1B). The mutant had increased abundances of EvgA, which mediates acid resistance, osmotic adaptation, and drug resistance and represses motility (55), as well as OmpR, which plays a central role in acid stress response and is involved in osmoregulation (56) (Table S1B). Additional evidence of the mutant's increased acid stress responses included increased abundance of glutamic acid decarboxylase regulator GadW and hydrolase PxpA, which consumes ATP to form L-glutamate (52) (Table S2). The abundance of enzymes that break down amino acids to release ammonium ions, which would acidify the cytoplasm, decreased in the Δ$trhA_{EC}$ mutant compared to the WT (Fig. 3C and D and Table S1A). Growth of the Δ$trhA_{EC}$ mutant, despite a depolarized membrane potential relative to the WT, is thus likely at the expense of reduced metabolism, motility, and expression of acid, alkaline, osmotic, and/or oxidative stress responses. These data also support that changes in the membrane potential, as reported here with fluorescent dyes, are relevant readouts to further probe the role of TrhA.

The Δ$trhA_{EC}$ mutant was less affected than the WT under stressful growth conditions. To test the hypotheses generated by the proteomics data described above, we compared the abilities of *E. coli* WT and the Δ$trhA_{EC}$ mutant to grow under acid, alkaline, and osmotic

stress. We did not test oxidative stress, since it is associated with acid or osmotic stresses (54). When exposed to acid stress, the Δ*trhA*$_{EC}$ mutant resumed logarithmic growth 6 h post-shift at pH 4.5, which was shorter than the 10-h delay for *E. coli* WT (Fig. 7A). The Δ*trhA*$_{EC}$ mutant grew faster than the WT at pH 4.5, and it reached a maximal optical density close to that of both the WT and Δ*trhA*$_{EC}$ at pH 7.0 (Fig. 7A). The fast growth of the mutant at pH 4.5 correlated with an increased $\Delta\psi$ relative to its $\Delta\psi$ at pH 7.0 (Fig. 7F). This pattern was opposite to the depolarization of the *E. coli* WT $\Delta\psi$ at pH 4.5 compared to pH 7.0 (Fig. 7F). When grown under alkaline stress (pH 9.0), the Δ*trhA*$_{EC}$ mutant had a shorter lag phase and grew faster and to a higher cell density than the WT (Fig. 7B). The maximal cell density of the mutant at alkaline pH remained low compared to growth at pH 7.0, indicating that the mutant still experienced stress, albeit not as severely as that WT (Fig. 7B). At pH 9.0, the $\Delta\psi$ of WT and Δ*trhA*$_{EC}$ strains became hyperpolarized (Fig. 7G), but the increase in $\Delta\psi$ was greater for the Δ*trhA*$_{EC}$ mutant strain than for the WT, consistent with the mutant's faster growth under these conditions (Fig. 7G). The mutant lacking TrhA is not able to adjust its membrane potential to levels similar to those of the WT when challenged with conditions causing proton gradient stress. The observations that the mutant's membrane potential is hyperpolarized under both acid and alkaline stress compared to the WT under similar conditions further suggest the that mutant is impaired in its ability to adjust membrane potential with changing conditions.

Next, we manipulated charge gradients through osmotic stress. In the presence of 0.75 M NaCl, the Δ*trhA*$_{EC}$ strain initiated growth roughly 5.5 h post-exposure to the stress, while *E. coli* WT began to grow after about 7 h (Fig. 7C). With 1.0 M NaCl, the mutant showed minimal slow growth after approximately 17 h post-stress exposure, while the *E. coli* WT did not grow (Fig. 7C). These differences are consistent with the mutant being preacclimated to osmotic stress suggested by proteomics. High concentrations of NaCl produced a similar growth defect in the *E. coli* WT and the Δ*trhA*$_{EC}$ mutant, with both strains reaching equivalent low maximum densities under these conditions, consistent with the two strains experiencing similar osmotic stress (Fig. 7C). Similar small growth advantages of the mutant relative to the WT were observed using KCl (Fig. 7D). There was no such preacclimation or growth advantage for the mutant relative to the WT when the uncharged sorbitol was used to provoke osmotic stress (Fig. 7E). These findings suggest the preacclimation of the mutant is specific to changes in the concentrations of protons or salt in the cells' environment.

Additional physiological changes of the Δ*trhAEC* mutant support a defective $\Delta\psi$. Cells with a perturbed membrane potential have pleiotropic defects, consistent with the central role of membrane potential in cellular physiology (57). Susceptibility to some antibiotics is associated with a perturbed membrane potential (57). The Δ*trhA*$_{EC}$ mutant was more resistant to antibiotics representing different mechanisms of action—protein (chloramphenicol and tetracycline) or cell wall (ampicillin) synthesis, membrane permeability (gramicidin D and filipin III), and membrane potential (nigericin and valinomycin) (Fig. 4C). One exception was polymyxin B, for which we did not detect any difference between the strains. The greatest differences between *E. coli* WT and the Δ*trhA*$_{EC}$ strain were for membrane pore-forming antibiotics (gramicidin D) and antibiotics targeting transmembrane ion gradients (nigericin and valinomycin). Membrane potential also affects the ability of cells to form and communicate within and between biofilms (13, 14), and we found that the Δ*trhA*$_{EC}$ strain produced roughly 1.5 times as much biofilm as *E. coli* WT (Fig. 4D). The pleiotropic phenotypes are consistent with TrhA's role in membrane energetics.

TrhA homologs in other bacteria function in membrane energetics homeostasis linked to FA metabolism. Given the conservation of TrhA homologs in several other bacteria, we speculated that their functions should also be conserved. Comparison of the $\Delta\psi$ of a different strain of *E. coli*, UB1005, and its derivative lacking TrhA (Δ*trhA*$_{UB}$) using ThT and $DiOC_2(3)$ indicated the Δ*trhA*$_{UB}$ mutant had a hyperpolarized $\Delta\psi$ relative to its parent, regardless of the reporter probe used (Fig. S5A and B). The hyperpolarized $\Delta\psi$ of the Δ*trhA*$_{UB}$ mutant, opposite to that of the mutant derivative of MG1655, was associated with reduced growth in the presence of acid, alkaline, or salt stresses, while

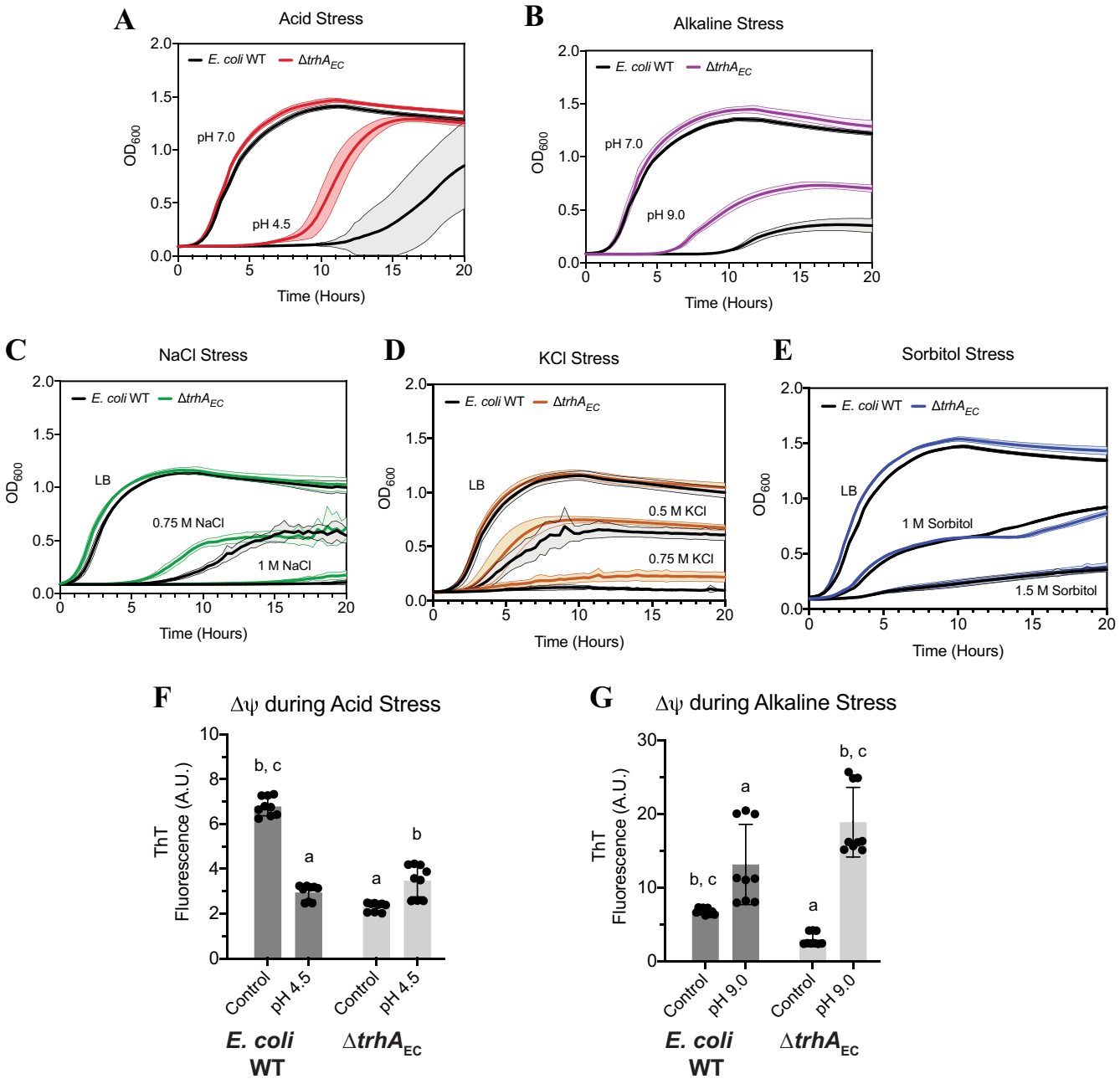

FIG 7 The Δ*trhA*$_{EC}$ mutant is preadapted to external stressors that perturb charge or ion gradients across the membrane. (A to E) *E. coli* WT and the Δ*trhA*$_{EC}$ mutant cells were grown to the logarithmic phase at 37°C in LB medium at pH 7.0 and then shifted to (A) acid stress at pH 4.5, (B) alkaline stress at pH 9.0, (C) NaCl stress at 0.75 M or 1 M NaCl, (D) KCl stress at 0.5 M or 0.75 M KCl, or (E) sorbitol stress at 1 M or 1.5 M sorbitol. All growth curves are representative of the average and standard deviation of three biological replicates with three technical replicates. (F and G) The membrane potential of *E. coli* WT and the Δ*trhA*$_{EC}$ mutant was measured using (F) ThT during acid stress at pH 4.5 or (G) alkaline stress at pH 9.0. All measurements represent the membrane potential measurements from three biological and three technical replicates. Error bars represent the standard deviation. a, significantly different from *E. coli* WT control ($P < 0.05$); b, significantly different from Δ*trhA*$_{EC}$ control ($P < 0.05$); c, significantly different from *E. coli* WT stress treatment (pH 4.5 or pH 9.0) ($P < 0.05$).

sorbitol had no apparent effect (Fig. S5C to G). Therefore, the deletion of *trhA* in UB1005 and MG1655 yields opposite effects on growth with protons or salt stress. This pattern of behavior is consistent with a dysregulated maintenance of membrane energetics in the mutant lacking TrhA relative to their parent strains and an inability of mutant cells to establish a WT-like membrane potential under given growth conditions. We refer to this mutant phenotype as a dysregulation of membrane potential homeostasis because *E. coli* strains lacking TrhA experience either a membrane de- or hyper-polarization relative to their parent under various growth

conditions. We do not yet know what provokes this opposite effect, but it is possible that the genetic background of UB1005 (harboring additional mutations in *relA* and *spoT* genes [58]) contributes to this difference.

We also characterized the role of the TrhA homolog (encoded by the *yplQ* gene) in the distantly related *Bacillus subtilis* strain 168 and a mutant derivative lacking the TrhA homolog ($\Delta trhA_{BS}$). Using two different reporter dyes, previously used to measure $\Delta\psi$ of *B. subtilis* (59), we showed that the resting $\Delta\psi$ of *B. subtilis* WT was higher (at least 50% more) than that of the $\Delta trhA_{BS}$ mutant (Fig. 8A and B). The findings indicate that $TrhA_{BS}$ supports its role in membrane potential homeostasis in *B. subtilis*.

To determine if the lack of $TrhA_{BS}$ also provoked changes in membrane FA composition, we compared the FA composition of the *B. subtilis* WT and $\Delta trhA_{BS}$ mutant membranes and found subtle differences at 37°C versus 16°C. At 37°C, the only differences were that the $\Delta trhA_{BS}$ mutant produced more C14:0 than *B. subtilis* WT (Fig. 8C). At 16°C, the $\Delta trhA_{BS}$ strain produced more C14:0 and fewer C17:1 anteisos than *B. subtilis* WT (Fig. 8D). Despite these changes, the $\Delta trhA_{BS}$ mutant made the same adjustments that *B. subtilis* WT made to its FA profile when acclimating from 37°C to 16°C (Fig. S6A and B), and net membrane fluidity was unaffected (Fig. 8E). Thus, mutants lacking *trhA* in *B. subtilis* and *E. coli* have similar subtle changes in their FA profiles. These changes are small yet consistent across the strains analyzed, suggesting that TrhA has some unknown, small effects on FA metabolism in both *E. coli* and *B. subtilis*.

DISCUSSION

Here, we present evidence that TrhA homologs, which are distantly related to eukaryotic PAQRs, are required for homeostasis of membrane energetics in two *E. coli* strains and in *B. subtilis* using defined mutants, physiological assays, and evaluation of membrane potential using fluorescent dye reporters as a read-out of membrane energetics status. The following lines of evidence support this conclusion: the bacterial mutant strains lacking TrhA homologs (i) possess a dysregulated membrane potential relative to the WT in *E. coli* and *B. subtilis* under various growth conditions, (ii) display either depolarized or hyperpolarized membrane potential relative to WT, (iii) show pleiotropic physiological changes consistent with dysregulated membrane energetics, and (iv) experience further depolarization or hyperpolarization in response to changes in proton or salt gradients in *E. coli*. Given the phylogenetic distance of *B. subtilis* and *E. coli*, control of membrane energetics homeostasis is the likely shared function of bacterial TrhA homologs.

The membrane proteomes of a $\Delta trhA_{EC}$ strain revealed concurrent physiological stresses and altered cellular metabolism, which suggested altered membrane energetics with dysregulated membrane potential homeostasis in the mutant relative to the WT, confirming these observations. Perturbation of the bacterial membrane potential is associated with drug potency (57), motility defects (60, 61), and an inability to achieve pH homeostasis (20). We observed each of these phenotypes for *E. coli* lacking $TrhA_{EC}$. Depolarized cells have destabilized membranes, protein mistranslation, and misfolding that is not severe enough to cause cell death (17), consistent with the $\Delta trhA_{EC}$ mutant's ability to grow similarly to the WT. Proteomics changes in the $\Delta trhA_{EC}$ mutant compared to the WT indicated that the mutant adjusts its metabolism and physiology to grow under laboratory conditions by reorganizing its metabolism to maintain essential transport and metabolic processes, minimizing transmembrane ions and metal fluxes and elevating cellular stress responses to charged molecules.

The cytoplasm of *E. coli* becomes acidified during acid and osmotic stress, and *E. coli* uses similar mechanisms to cope with these stressors (62). Altered acid, alkaline, and salt stress responses compared to parent strains were observed in both $\Delta trhA_{EC}$ and $\Delta trhA_{UB}$. Exposure to acidic pH decreases the PMF of *E. coli* and depolarizes the $\Delta\psi$ (63). Exposure to external high pH artificially increases the PMF of *E. coli* WT and hyperpolarizes the $\Delta\psi$ (64). Here, we observed similar $\Delta\psi$ changes for the *E. coli* MG1655 strain. However, the $\Delta\psi$ of $\Delta trhA_{EC}$ became hyperpolarized under both high

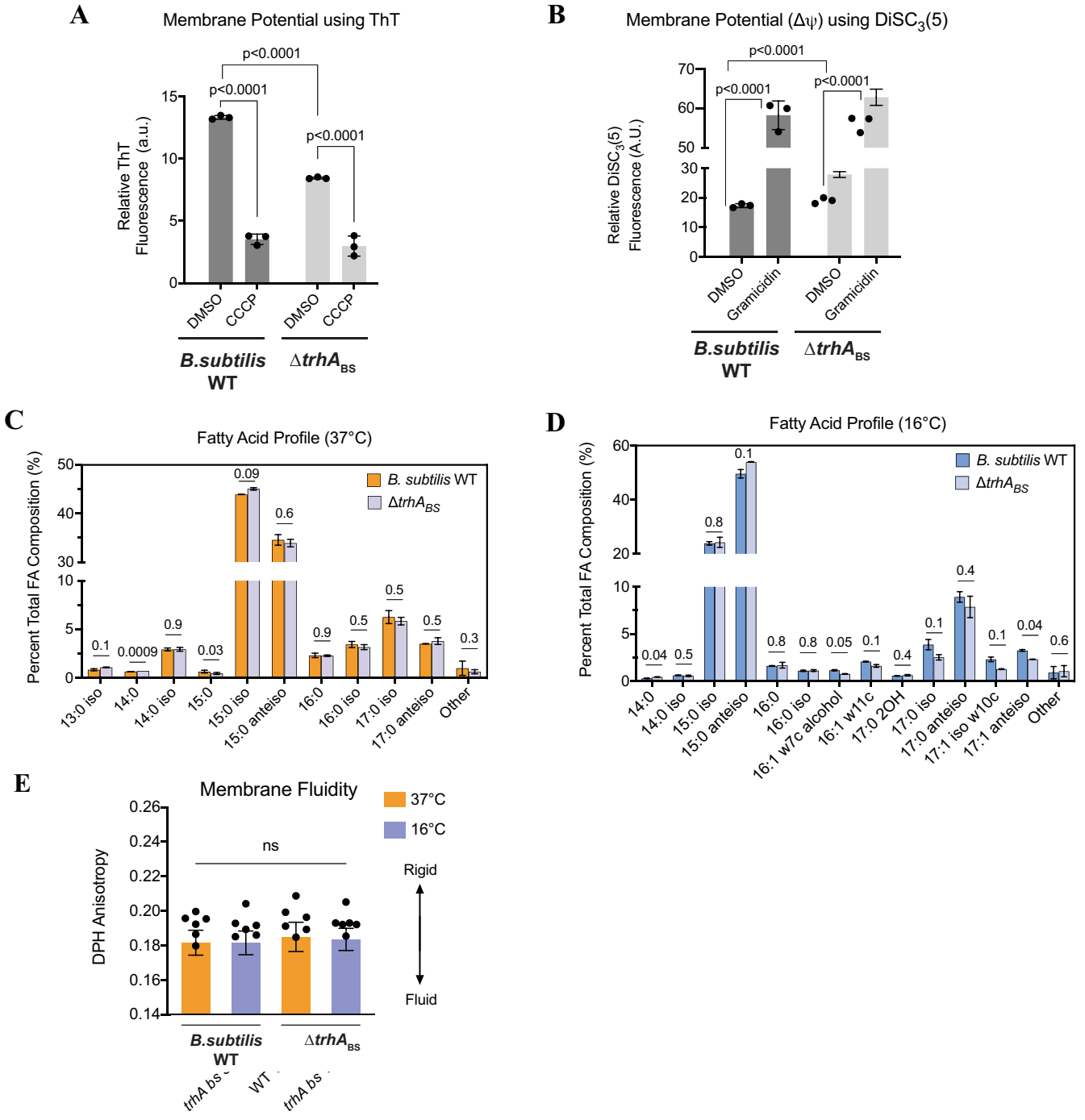

FIG 8 The TrhA homolog in *Bacillus subtilis* affects membrane potential. (A) Membrane potential measurements of *B. subtilis* WT and the Δ*trhA*$_{BS}$ strain using ThT reporter. DMSO treatments represent the resting membrane potential of cells. The membrane potential of each strain was collapsed when treated with CCCP, as indicated by a decrease in fluorescence of ThT relative to that of the DMSO control. Data are representative of a single experiment, with one biological replicate and three technical replicates. (B) Membrane potential measurements of *B. subtilis* WT and the Δ*trhA*$_{BS}$ mutant using DiSC3 (5) reporter. Fluorescence of the polar, hydrophobic DiSC3(5) dye is quenched as it enters polarized cells. Because CCCP is incompatible for use with $DiSC_3(5)$ in this assay (58), we used gramicidin D to depolarize $\Delta\psi$. Upon membrane depolarization using gramicidin, DiSC3(5) is released back into the free medium, and fluorescence is dequenched. The data are representative of a single experiment, with one biological replicate and three technical replicates. (C) Total fatty acid composition of *B. subtilis* WT and the Δ*trhA*$_{BS}$ strain grown at 37°C. (D) Total fatty acid composition of *B. subtilis* WT and the Δ*trhA*$_{BS}$ strain grown at 16°C. Error bars represent the standard deviation of two biological and two technical replicates. *P* values are listed above each set of bars. (E) Membrane fluidities of *B. subtilis* WT and the Δ*trhA*$_{BS}$ strain grown at 37°C and 16°C. Membrane fluidity of whole cells was measured using DPH anisotropy, where higher values in anisotropy indicate a more rigid membrane. Data represent six biological replicates, where each point is the average of three technical replicates. Error bars represent the standard deviation.

and low external pH conditions. The mutant response is consistent with altered membrane potential homeostasis (i.e., WT-like) in Δ*trhA*$_{EC}$. Changes in external pH or salt concentrations led to reduced growth for both WT and mutant pairs. However, under these conditions, growth of Δ*trhA*$_{EC}$ was greater than its parent, while growth of Δ*trhA*$_{UB}$ was further reduced compared to its parent. These responses tracked the depolarized (Δ*trhA*$_{EC}$) or hyperpolarized (Δ*trhA*$_{UB}$) $\Delta\psi$ of these mutants compared to their parents. We surmise that low or high external pH and high salts conditions artificially further increase (Δ*trhA*$_{EC}$) or decrease (Δ*trhA*$_{UB}$) the ΔpH and/or $\Delta\psi$ of the mutants compared to parent strains. While we do not know how these opposite effects are produced, these responses are consistent with our hypothesis that the mutants have an altered ability to maintain membrane potential homeostasis.

We do not yet know the mechanism(s) by which TrhA modulates membrane potential homeostasis in bacteria. However, the data obtained here, combined with information available from distant eukaryotic homologs, hint at a possible mechanism(s) to be investigated in the future. Eukaryotic class I PAQRs from humans and *C. elegans* control the abundances of unsaturated FAs in the membrane in response to conditions that decrease membrane fluidity, such as low temperature or dietary fatty acids (27–30, 41–43, 45). Our study demonstrates that the bacterial TrhA (PAQR class III) homologs do *not* primarily control membrane fluidity. However, our data suggest a role for TrhA in FA metabolism. TrhA$_{EC}$ is part of the FabR regulon and is expressed similarly to *fabAB*, implying that TrhA$_{EC}$ is expressed under conditions where long unsaturated FAs are produced. The FA profiles of mutants lacking TrhA in both *E. coli* and *B. subtilis* have small but consistent changes relative to parent strains—reduction in abundance of long, unsaturated FAs and accumulation of short, saturated FAs. Furthermore, PAQR family proteins are found in *Bacteria* phyla in which membranes include ester-linked fatty acids, but not in *Archaea* (24) with isoprenoid lipids (65). Membrane lipids are essential to membrane protein folding and function (4). In the absence of a molecular mechanism, we cannot dissociate whether the dysregulated membrane potential which occurs with a lack of TrhA is through changes in membrane protein abundances, suggested by proteomics data for the MG1655 and mutant pair, or whether it is associated with an effect of TrhA on membrane FA composition, which was observed for both *E. coli* strains and *B. subtilis* WT and mutant pairs analyzed here. Based on the evidence here, together with the role of distantly related eukaryotic PAQRs known to date and the phylogenetic distribution of TrhA bacterial homologs, we favor the hypothesis that TrhA homologs mediate their effect on membrane potential homeostasis through their effect on unsaturated FA metabolism.

The protein sequence of bacterial TrhA homologs and of the most closely related class III eukaryotic PAQRs are significantly shorter than other eukaryotic PAQR homologs from classes I and II studied to date (24). The longer eukaryotic homologs may thus have evolved divergent functions relative to the ancestral class III homologs, such as binding ligands such as adiponectin or modulating membrane fluidity. The findings here lead us to propose that a common function of PAQR family proteins is homeostasis of the membrane (membrane fluidity or energetics) linked to fatty acid metabolism.

MATERIALS AND METHODS

Strains and media. The bacterial strains used in this study are listed in Table 1. *E. coli* and *B. subtilis* strains were grown at 37°C in Luria broth (LB), minimal M9 medium containing glucose or oleate, or on LB agar plates supplemented with antibiotics (100 μg/mL ampicillin, 34 μg/mL chloramphenicol, or 50 μg/mL kanamycin). Inducers were used at 1 mM IPTG (isopropyl β-D-1-thiogalactopyranoside) (pRH005 and pTrc99a) or 1% L-arabinose (pBAD33). The Δ*trhA* strain derivatives of *E. coli* MG1655 and UB1005 were generated by Lambda-red recombination (66). *Bacillus subtilis* 168 and the Δ*trhA*$_{BS}$ strain were obtained from the *Bacillus* Genetic Stock Center (BGSC).

Plasmid construction and genome sequencing. The pUA66, pUA-*trhA*$_{EC}$, pUA-*fabA*, and pUA-*fabB* plasmids were obtained from the library of *E. coli* promoters fused to GFP coding sequence (39) or constructed previously (66). PCR site-directed mutagenesis using primers *trhA*$_{EC}$ mut FabR site forward (Fwd) and *trhA*$_{EC}$ mut FabR site reverse (Rev) (Table 1) was used to mutate the FabR binding box in the *trhA*$_{EC}$ promoter. Plasmid pUA66 was modified for translational fusion by introducing the TAP tag sequence from plasmid pJL72 (67). The sequence of *trhA*$_{EC}$ (natural promoter and coding sequence) was introduced

TABLE 1 List of bacterial strains, plasmids, and primers used in this study[a]

Strain, plasmid, or primer	Relevant properties	Reference or source
Strains		
Escherichia coli MG1655	*F-*, *λ-*, *ilvG-*, *rfb-50*, *rph-1*	76
Δ*trhA*$_{EC}$	*F-*, *λ-*, *ilvG-*, *rfb-50*, *rph-1*, Δ*trhA*$_{EC}$::*Km*	This work
Δ*fadR*	*F-*, *λ-*, *ilvG-*, *rfb-50*, *rph-1*, Δ*fadR*	67
Δ*fadR*Δ*fabR*	P1 transduction of Δ*fabR*::*Km* (Keio collection) in Δ*fadR*. Km cassette removed using pCP20 plasmid.	This work
MG1655 (pRH005)	MG1655 containing empty (pRH005) (Km, Cm)	This work
Δ*trhA*$_{EC}$ (pRH005)	Δ*trhA*$_{EC}$ containing empty (pRH005) (Km, Cm)	This work
Δ*trhA*$_{EC}$ (pRH005 *trhA*$_{EC}$)	Δ*trhA*$_{EC}$ containing (pRH005 *trhA*$_{EC}$) (Km, Cm)	This work
MG1655 (pBAD33)	MG1655 containing empty (pBAD33) (Cm)	This work
Δ*trhA*$_{EC}$ (pBAD33)	Δ*trhA*$_{EC}$ containing empty (pBAD33) (Cm)	This work
Δ*trhA*$_{EC}$ (pBAD33 *trhA*$_{EC}$)	Δ*trhA*$_{EC}$ containing (pBAD33 *trhA*$_{EC}$) (Cm)	This work
MG1655 (pTrc99a)	MG1655 containing empty (pTrc99a) (Ap)	This work
Δ*trhA*$_{EC}$ (pTrc99a)	Δ*trhA*$_{EC}$ containing empty (pTrc99a) (Ap)	This work
Δ*trhA*$_{EC}$ (pTrc99a *trhA*$_{EC}$)	Δ*trhA*$_{EC}$ containing (pTrc99a *trhA*$_{EC}$), (Ap)	This work
Escherichia coli Top10	General cloning strain	Invitrogen
Escherichia coli UB1005	F-, *λ-*, *gyrA37*(NalR), *relA1*, *spoT1*, *metB1*, *λ*^{R}	77
UB1005 Δ*trhA*$_{EC}$	F-, *λ-*, *gyrA37*(NalR), *relA1*, *spoT1*, *metB1*, *λ*^{R}, Δ*trhA*::*Km*	This work
Bacillus subtilis 168	*trpC2*	78; BGSC
Δ*trhA*$_{BS}$	*trpC2*, Δ*yplQ*::*Erm*	78; BGSC
Plasmids		
pUA66	ori sc101, GFPmut2 (Km)	40
pUA-*fabB*	*fabB* promoter in pUA66	67
pUA-*fabA*	*fabA* promoter in pUA66	67
pUA-*trhA*$_{EC}$	*trhA*$_{EC}$ promoter in pUA66	40
pUA-*trhA*$_{EC}$mut	Site-directed PCR mutagenesis in the FabR binding site on the pUA- *trhA*$_{EC}$ plasmid	This work
pJL72	TAP tag sequence	68
pUA-TAP	TAP tag sequence from pJL72 (BamHI/EcoRV) in pUA66 (BamHI/HincII)	This work
pUA-TrhA$_{EC}$-TAP	*trhA*$_{EC}$ gene (promoter and ORF) cloned in phase with TAP sequence in pEB1588(XhoI/BamHI)	This work
pDONR221	Gateway-based cloning vector (Km)	Invitrogen
pRH005	Gateway-based destination vector expressing proteins fused with YFP at the C terminus; ori RK2*oriV*, (Km, Cm)	51
pRH005 *trhA*$_{EC}$	pRH005 containing WT *trhA*$_{EC}$, (Km, Cm)	This work
pTrc99a	Expression vector with inducible LacI promoter; ori ColE1/pMB1/pBR322, (Ap)	79
pTrc99a *trhA*$_{EC}$	pTrc99a containing *trhA*$_{EC}$ (Cm)	This work
pBAD33	Expression vector with arabinose-inducible promoter; ori pACYC184/p15A (Cm)	80
pBAD33 *trhA*$_{EC}$	pBAD33 containing *trhA*$_{EC}$ (Cm)	This work
Primers		
trhA$_{EC}$ Fwd	CACCATGGTTCAGAAGCCCCTC	
trhA$_{EC}$ Rev	TTACGCCTGCCCAATATA	
UP *trhA*$_{EC}$ XhoI	ttgctcgagGAAAATATGACCCTGACTGAACTG	
trhA$_{EC}$ BamHI Rev	cgggatccCGCCTGCCCAATATACAAATAGATC	
trhA$_{EC}$mut FabR site Fwd	CAGAATTTATTTTAGCTAGTGGGTGTTCACTGGAAC	
trhA$_{EC}$mut FabR site Rev	GTTCCAGTGAACACCCACTAGCTAAAATAAATTCTG	
GW *trhA*$_{EC}$ Fwd	GGGGACAAGTTTGTACAAAAAAGCAGGCTATGGTTCAGAAGCCCCTCATT	
GW *trhA*$_{EC}$ Rev	GGGGACCACTTTGTACAAGAAAGCTGGGTCCGCCTGCCCAATATACAA	
GW *pgk* Fwd	GGGGACAAGTTTGTACAAAAAAGCAGGCTATGTCTGTAATTAAGATGACC	
GW *pgk* Rev	GGGGACCACTTTGTACAAGAAAGCTGGGTCCTTCTTAGCGC GCTCTTC	
pRH005 *ccdB* mut Fwd	ATGTTCTAAAGCAGGTAAATGTCAGGC	
pRH005 *ccdB* mut Rev	GCCTGACATTTACCTGCTTTAGAACAT	
XbaI *trhA*$_{EC}$ Fwd	TAAGCATCTAGATCTAGGAGGTAAGTTATGGTT	
HindIII *trhA*$_{EC}$ Rev	TGCTTAAAGCTTTTACGCCTGCCCAATATA	

[a]Km, kanamycin; Cm, chloramphenicol; Ap, ampicillin; Erm, erythromycin; BGSC, *Bacillus* Genetic Stock Center. The restriction enzymes used are underlined as part of the primer name, and the location of these restriction sites within the primer is underlined.

using the XhoI and BamHI sites of pUA66. Gateway technology, as per the manufacturer's protocol (Invitrogen), was used to clone into pRH005 (51) (Table 1). Cloning in the pTrc99a and pBAD33 plasmids (Table 1) was completed by restriction digestions and ligation using primers XbaI *trhA*$_{EC}$ Fwd and HindIII *trhA*$_{EC}$ Rev (Table 1). All plasmids were sequence-verified before being introduced into *E. coli* by transformation. The genomes of the *E. coli* MG1655 and Δ*trhA*$_{EC}$ strains were sequenced at the Microbial Genome Sequencing Center (MiGS; Pittsburgh, PA, USA).

Transcriptional fusion analysis. Transcriptional GFP fusions in the Δ*fadR* and Δ*fadR*Δ*fabR E. coli* strains were done as described in reference 67.

SDS-PAGE and Western blotting. Total cell extracts were prepared by resuspending cell pellets in Laemmli buffer 1× at a concentration of 0.3 optical density at 600 nm (OD_{600}) in 10 μL (we did not heat, as we observed that this prevents correct migration/detection of the integral TrhA protein in SDS-PAGE), followed by electrotransfer onto nitrocellulose membranes. TrhA-TAP-tagged protein was detected with peroxidase-antiperoxidase antibodies (Sigma) and colorimetric, detection with diaminobenzidine.

Fatty acid methyl ester (FAME) analysis. Whole-cell FAME analysis of *E. coli* and *B. subtilis* was done by gas chromatography-mass spectrometry (GC-MS) through Microbial ID (Newark, DE) using cultures grown at 37°C or 16°C to early stationary phases (OD_{600} of 1.5 to 2.0).

DPH anisotropy. The fluorescent dye DPH (1,6-diphenyl-1,3,5-hexatriene) was used to measure anisotropy, as described previously (46).

Membrane Proteomics. Membrane protein fractions were prepared as described in reference 68. Bacterial cell membrane proteins were denatured, reduced, alkylated, and enzymatically digested into peptides using previously established methods (69, 70). All samples were analyzed on a Q Exactive Plus mass spectrometer (Thermo Fisher Scientific) coupled with a Proxeon EASY-nLC 1200 liquid chromatography (LC) pump (Thermo Fisher Scientific). Peptides were separated on a 75-μm inner diameter microcapillary column packed with 30 cm of Kinetex C_{18} resin (1.7 μm, 100 Å; Phenomenex) that was heated to 60°C in a Phoenix S&T NanoLC column heater. For each sample, 2- μg aliquots of peptides were loaded in buffer A (0.1% formic acid, 2% acetonitrile) and eluted with a linear 210-min organic gradient followed by a wash and column reequilibration as follows: 0% to 2% solvent B over 27 min, 2% to 25% solvent B over 148 min, 25% to 50% solvent B over 10 min, 50% to 0% solvent B over 10 min, hold at 0% solvent B for 15 min. The flow rate was kept at 200 nL/min. MS data were acquired with Thermo Xcalibur software v4.27.19 using the topN method, where N can be up to 10.

Data were processed in Proteome Discoverer v2.3 (Thermo Scientific) using MS Amanda v2.0 (71) and Percolator (72). Spectral data were searched against the *E. coli* reference proteome database, and common laboratory contaminants and identifications were controlled at a false-discovery rate (FDR) of <1% at the peptide level. Proteins were quantified according to the sum of their peptide chromatographic areas under the curve and normalized in Proteome Discoverer by the total peptide amount. To identify differential protein abundances, hypothesis testing was performed by *t* tests, and adjusted *P* values were calculated based on the background population of proteins. Log_2 protein abundance differences were determined to assess the fold change. Proteins were assigned to appropriate Gene Ontology (GO) term categories using EcoCyc. These data are available in the ProteomeXchange Consortium via the MASSIVE repository (https://massive.ucsd.edu/; username, MSV000088025_reviewer; password, ecoli_membrane).

Measurement of $\Delta\psi$ using $DiOC_2(3)$, ThT, and $DiSC_3(5)$. Colonies of *E. coli* and *B. subtilis* were grown overnight at 37°C in LB broth, reinoculated (250 μL into 3 mL of fresh LB), and shaken for 2.5 h at 37°C. Membrane potential was measured as described (59, 73).

Physiological assays. Growth of *E. coli* was determined in 200 μL of LB in a 96-well plate with shaking using an ELx808 absorbance microplate reader (Biotek). The specific growth rate, μ, was calculated as described (74). The ATP concentration was quantified using the BacTiter-Glo kit luminescence assay as per the manufacturer's protocol (Promega). Biofilms were quantified as described (75).

For soft agar assays, five5 μL of culture was inoculated into the center of plates containing terrific broth (TB) (12 g/L tryptone, 10 g/L yeast extract, 0.4% glycerol [vol/vol]), 10% 1× phosphate-buffered saline [PBS]) with 0.3% agar (wt/vol). Plates were incubated for 15 h at 28°C.

For acid, alkaline, and osmotic stress tests, the pH of Luria Broth (LB) was adjusted to 4.5, 7.0, or 9.0 using HCl or NaOH or supplemented with 0.75 and 1 M for NaCl, 1.0 M and 1.5 M Sorbitol, and 0.5 M and 0.75 M KCl. Growth in stress conditions was determined as described above.

For MICs, cells were grown in LB to the log phase, diluted in 200 μL of fresh LB containing antibiotics at concentrations denoted in Fig. 4C, and shaken overnight using an ELx808 absorbance microplate reader (Biotek). Concentration (MIC) values were determined by the lowest antibiotic concentration added to the medium at which the growth rate was inhibited.

Statistical analyses. Statistical analyses were performed in GraphPad Prism 9. Two-tailed *t* tests were applied for normally distributed data with one degree of freedom. Exact *n* values are provided in each figure. Representative images or results are shown for soft agar motility assays and $DiSC_3(5)$, where experiments were repeated at least three times.

SUPPLEMENTAL MATERIAL

Supplemental material is available online only.

SUPPLEMENTAL FILE 1, PDF file, 6.8 MB.

ACKNOWLEDGMENTS

This research is supported by National Science Foundation grant NSF-MCB 1715185 (to R.L.H. and G.A.), National Science Foundation grant NSF-IOS 1855066 (to G.A.), a Dr. Donald L. Akers, Jr., Faculty Enrichment award (to G.A.), and a UT research seed award (to G.A.). Any opinions, findings, conclusions, or recommendations expressed in this

material are those of the authors and do not necessarily reflect the views of the National Science Foundation.

We acknowledge Lam Vo for assistance with the initial analysis of membrane proteomics data and Neyland Harmon and Morgan House for technical assistance on membrane potential measurements.

REFERENCE

1. Zhang YM, Rock CO. 2008. Membrane lipid homeostasis in bacteria. Nat Rev Microbiol 6:222–233. https://doi.org/10.1038/nrmicro1839.
2. Sohlenkamp C, Geiger O. 2016. Bacterial membrane lipids: diversity in structures and pathways. FEMS Microbiol Rev 40:133–159. https://doi.org/10.1093/femsre/fuv008.
3. Casares D, Escribá PV, Rosselló CA. 2019. Membrane lipid composition: effect on membrane and organelle structure, function and compartmentalization and therapeutic avenues. Int J Mol Sci 20:2167. https://doi.org/10.3390/ijms20092167.
4. Bogdanov M, Mileykovskaya E, Dowhan W. 2008. Lipids in the assembly of membrane proteins and organization of protein supercomplexes: implications for lipid-linked disorders. Subcell Biochem 49:197–239. https://doi.org/10.1007/978-1-4020-8831-5_8.
5. Rowlett VW, Mallampalli VK, Karlstaedt A, Dowhan W, Taegtmeyer H, Margolin W, Vitrac H. 2017. Impact of membrane phospholipid alterations in Escherichia coli on cellular function and bacterial stress adaptation. J Bacteriol 199:e00849-16. https://doi.org/10.1128/JB.00849-16.
6. Levental KR, Malmberg E, Symons JL, Fan YY, Chapkin RS, Ernst R, Levental I. 2020. Lipidomic and biophysical homeostasis of mammalian membranes counteracts dietary lipid perturbations to maintain cellular fitness. Nat Commun 11:1–13. https://doi.org/10.1038/s41467-020-15203-1.
7. Fadeel B, Xue D. 2009. The ins and outs of phospholipid asymmetry in the plasma membrane: roles in health and disease. Crit Rev Biochem Mol Biol 44:264–277. https://doi.org/10.1080/10409230903193307.
8. Bogdanov M, Pyrshev K, Yesylevskyy S, Ryabichko S, Boiko V, Ivanchenko P, Kiyamova R, Guan Z, Ramseyer C, Dowhan W. 2020. Phospholipid distribution in the cytoplasmic membrane of Gram-negative bacteria is highly asymmetric, dynamic, and cell shape-dependent. Sci Adv 6:eaaz6333. https://doi.org/10.1126/sciadv.aaz6333.
9. Aguilar PS, De Mendoza D. 2006. Control of fatty acid desaturation: a mechanism conserved from bacteria to humans. Mol Microbiol 62:1507–1514. https://doi.org/10.1111/j.1365-2958.2006.05484.x.
10. De Mendoza D, Pilon M. 2019. Control of membrane lipid homeostasis by lipid-bilayer associated sensors: a mechanism conserved from bacteria to humans. Prog Lipid Res 76:100996. https://doi.org/10.1016/j.plipres.2019.100996.
11. Benarroch JM, Asally M. 2020. The microbiologist's guide to membrane potential dynamics. Trends Microbiol 28:304–314. https://doi.org/10.1016/j.tim.2019.12.008.
12. Abdul Kadir L, Stacey M, Barrett-Jolley R. 2018. Emerging roles of the membrane potential: action beyond the action potential. Front Physiol 9:1661. https://doi.org/10.3389/fphys.2018.01661.
13. Prindle A, Liu J, Asally M, Ly S, Garcia-Ojalvo J, Süel GM. 2015. Ion channels enable electrical communication in bacterial communities. Nature 527:59–63. https://doi.org/10.1038/nature15709.
14. Humphries J, Xiong L, Liu J, Prindle A, Yuan F, Arjes HA, Tsimring L, Süel GM. 2017. Species-independent attraction to biofilms through electrical signaling. Cell 168:200–209. https://doi.org/10.1016/j.cell.2016.12.014.
15. Lee D-YD, Galera-Laporta L, Bialecka-Fornal M, Moon EC, Shen Z, Briggs SP, Garcia-Ojalvo J, Süel GM. 2019. Magnesium flux modulates ribosomes to increase bacterial survival. Cell 177:352–360. https://doi.org/10.1016/j.cell.2019.01.042.
16. Liu J, Martinez-Corral R, Prindle A, Lee D-YD, Larkin J, Gabalda-Sagarra M, Garcia-Ojalvo J, Süel GM. 2017. Coupling between distant biofilms and emergence of nutrient time-sharing. Science 356:638–642. https://doi.org/10.1126/science.aah4204.
17. Bruni GN, Weekley RA, Dodd BJ, Kralj JM. 2017. Voltage-gated calcium flux mediates Escherichia coli mechanosensation. Proc Natl Acad Sci U S A 114:9445–9450. https://doi.org/10.1073/pnas.1703084114.
18. Payandeh J, Minor DL Jr. 2015. Bacterial voltage-gated sodium channels (BacNaVs) from the soil, sea, and salt lakes enlighten molecular mechanisms of electrical signaling and pharmacology in the brain and heart. J Molecular Biology 427:3–30. https://doi.org/10.1016/j.jmb.2014.08.010.
19. Furini S, Domene C. 2018. Ion-triggered selectivity in bacterial sodium channels. Proc Natl Acad Sci U S A 115:5450–5455. https://doi.org/10.1073/pnas.1722516115.
20. Krulwich TA, Sachs G, Padan E. 2011. Molecular aspects of bacterial pH sensing and homeostasis. Nat Rev Microbiol 9:330–343. https://doi.org/10.1038/nrmicro2549.
21. Doerrler WT, Sikdar R, Kumar S, Boughner LA. 2013. New functions for the ancient DedA membrane protein family. J Bacteriol 195:3–11. https://doi.org/10.1128/JB.01006-12.
22. Farha MA, Verschoor CP, Bowdish D, Brown ED. 2013. Collapsing the proton motive force to identify synergistic combinations against Staphylococcus aureus. Chem Biol 20:1168–1178. https://doi.org/10.1016/j.chembiol.2013.07.006.
23. Bezanilla F. 2008. How membrane proteins sense voltage. Nat Rev Mol Cell Biol 9:323–332. https://doi.org/10.1038/nrm2376.
24. Tang YT, Hu T, Arterburn M, Boyle B, Bright JM, Emtage PC, Funk WD. 2005. PAQR proteins: a novel membrane receptor family defined by an ancient7-transmembrane pass motif. J Mol Evol 61:372–380. https://doi.org/10.1007/s00239-004-0375-2.
25. Kupchak BR, Garitaonandia I, Villa NY, Smith JL, Lyons TJ. 2009. Antagonism of human adiponectin receptors and their membrane progesterone receptor paralogs by TNFα and a ceramidase inhibitor. Biochemistry 48:5504–5506. https://doi.org/10.1021/bi9006258.
26. Yamauchi T, Kamon J, Ito Y, Tsuchida A, Yokomizo T, Kita S, Sugiyama T, Miyagishi M, Hara K, Tsunoda M, Murakami K, Ohteki T, Uchida S, Takekawa S, Waki H, Tsuno NH, Shibata Y, Terauchi Y, Froguel P, Tobe K, Koyasu S, Taira K, Kitamura T, Shimizu T, Nagai R, Kadowaki T. 2003. Cloning of adiponectin receptors that mediate antidiabetic metabolic effects. Nature 423:762–769. https://doi.org/10.1038/nature01705.
27. Svensk E, Ståhlman M, Andersson CH, Johansson M, Borén J, Pilon M. 2013. PAQR-2 regulates fatty acid desaturation during cold adaptation in C. elegans. PLoS Genet 9:e1003801. https://doi.org/10.1371/journal.pgen.1003801.
28. Svensk E, Devkota R, Ståhlman M, Ranji P, Rauthan M, Magnusson F, Hammarsten S, Johansson M, Borén J, Pilon M. 2016. Caenorhabditis elegans PAQR-2 and IGLR-2 protect against glucose toxicity by modulating membrane lipid composition. PLoS Genet 12:e1005982. https://doi.org/10.1371/journal.pgen.1005982.
29. Devkota R, Svensk E, Ruiz M, Ståhlman M, Borén J, Pilon M. 2017. The adiponectin receptor AdipoR2 and its Caenorhabditis elegans homolog PAQR-2 prevent membrane rigidification by exogenous saturated fatty acids. PLoS Genet 13:e1007004. https://doi.org/10.1371/journal.pgen.1007004.
30. Bodhicharla R, Devkota R, Ruiz M, Pilon M. 2018. Membrane fluidity is regulated cell nonautonomously by Caenorhabditis elegans PAQR-2 and its mammalian homolog AdipoR2. Genetics 210:189–201. https://doi.org/10.1534/genetics.118.301272.
31. Thomas P. 2008. Characteristics of membrane progestin receptor alpha (mPRα) and progesterone membrane receptor component 1 (PGMRC1) and their roles in mediating rapid progestin actions. Front Neuroendocrinol 29:292–312. https://doi.org/10.1016/j.yfrne.2008.01.001.
32. Zhu Y, Rice CD, Pang Y, Pace M, Thomas P. 2003. Cloning, expression, and characterization of a membrane progestin receptor and evidence it is an intermediary in meiotic maturation of fish oocytes. Proc Natl Acad Sci U S A 100:2231–2236. https://doi.org/10.1073/pnas.0336132100.
33. Zhu Y, Bond J, Thomas P. 2003. Identification, classification, and partial characterization of genes in humans and other vertebrates homologous to a fish membrane progestin receptor. Proc Natl Acad Sci U S A 100:2237–2242. https://doi.org/10.1073/pnas.0436133100.
34. Baida GE, Kuzmin NP. 1996. Mechanism of action of hemolysin III from Bacillus cereus. Biochim Biophys Acta 1284:122–124. https://doi.org/10.1016/S0005-2736(96)00168-X.

35. Chen YC, Chang MC, Chuang YC, Jeang CL. 2004. Characterization and virulence of hemolysin III from Vibrio vulnificus. Curr Microbiol 49:175–179.
36. Feng Y, Cronan JE. 2011. Complex binding of the FabR repressor of bacterial unsaturated fatty acid biosynthesis to its cognate promoters. Mol Microbiol 80:195–218. https://doi.org/10.1111/j.1365-2958.2011.07564.x.
37. McCue LA, Thompson W, Carmack CS, Ryan MP, Liu JS, Derbyshire V, Lawrence CE. 2001. Phylogenetic footprinting of transcription factor binding sites in proteobacterial genomes. Nucleic Acids Res 29:774–782. https://doi.org/10.1093/nar/29.3.774.
38. Thomason MK, Bischler T, Eisenbart SK, Förstner KU, Zhang A, Herbig A, Nieselt K, Sharma CM, Storz G. 2015. Global transcriptional start site mapping using differential RNA sequencing reveals novel antisense RNAs in Escherichia coli. J Bacteriol 197:18–28. https://doi.org/10.1128/JB.02096-14.
39. Zhu K, Zhang YM, Rock CO. 2009. Transcriptional regulation of membrane lipid homeostasis in Escherichia coli. J Biological Chemistry 284: 34880–34888. https://doi.org/10.1074/jbc.M109.068239.
40. Zaslaver A, Bren A, Ronen M, Itzkovitz S, Kikoin I, Shavit S, Liebermeister W, Surette MG, Alon U. 2006. A comprehensive library of fluorescent transcriptional reporters for Escherichia coli. Nat Methods 3:623–628. https://doi.org/10.1038/nmeth895.
41. Holland WL, Miller RA, Wang ZV, Sun K, Barth BM, Bui HH, Davis KE, Bikman BT, Halberg N, Rutkowski JM, Wade MR, Tenorio VM, Kuo M-S, Brozinick JT, Zhang BB, Birnbaum MJ, Summers SA, Scherer PE. 2011. Receptor-mediated activation of ceramidase activity initiates the pleiotropic actions of adiponectin. Nat Med 17:55–63. https://doi.org/10.1038/nm.2277.
42. Pei J, Millay DP, Olson EN, Grishin NV. 2011. CREST: a large and diverse superfamily of putative transmembrane hydrolases. Biol Direct 6:37. https://doi.org/10.1186/1745-6150-6-37.
43. Vasiliauskaité-Brooks I, Sounier R, Rochaix P, Bellot G, Fortier M, Hoh F, De Colibus L, Bechara C, Saied EM, Arenz C, Leyrat C, Granier S. 2017. Structural insights into adiponectin receptors suggest ceramidase activity. Nature 544:120–123. https://doi.org/10.1038/nature21714.
44. Devkota R, Henricsson M, Borén J, Pilon M. 2021. The C. elegans PAQR-2 and IGLR-2 membrane homeostasis proteins are uniquely essential for tolerating dietary saturated fats. Biochim Biophys Acta 1866:158883. https://doi.org/10.1016/j.bbalip.2021.158883.
45. Ruiz M, Ståhlman M, Borén J, Pilon M. 2019. AdipoR1 and AdipoR2 maintain membrane fluidity in most human cell types and independently of adiponectin. J Lipid Res 60:995–1004. https://doi.org/10.1194/jlr.M092494.
46. Xu Y, Zhao Z, Tong W, Ding Y, Liu B, Shi Y, Wang J, Sun S, Liu M, Wang Y, Qi Q, Xian M, Zhao G. 2020. An acid-tolerance response system protecting exponentially growing Escherichia coli. Nat Commun 11:1496. https://doi.org/10.1038/s41467-020-15350-5.
47. Van de Vossenberg JL, Driessen AJ, da Costa MS, Konings WN. 1999. Homeostasis of the membrane proton permeability in Bacillus subtilis grown at different temperatures. Biochim Biophys Acta 1419:97–104. https://doi.org/10.1016/S0005-2736(99)00063-2.
48. Ashburner M, Ball CA, Blake JA, Botstein D, Butler H, Cherry JM, Davis AP, Dolinski K, Dwight SS, Eppig JT, Harris MA, Hill DP, Issel-Tarver L, Kasarskis A, Lewis S, Matese JC, Richardson JE, Ringwald M, Rubin GM, Sherlock G. 2000. Gene Ontology: tool for the unification of biology. Nat Genet 25: 25–29. https://doi.org/10.1038/75556.
49. Ehrenberg B, Montana V, Wei MD, Wuskell JP, Loew LM. 1988. Membrane potential can be determined in individual cells from the nernstian distribution of cationic dyes. Biophys J 53:785–794. https://doi.org/10.1016/S0006-3495(88)83158-8.
50. Mancini L, Terradot G, Tian T, Pu Y, Li Y, Lo C-J, Bai F, Pilizota T. 2020. A general workflow for characterization of Nernstian dyes and their effects on bacterial physiology. Biophys J 118:4–14. https://doi.org/10.1016/j.bpj.2019.10.030.
51. Hallez R, Letesson JJ, Vandenhaute J, De Bolle X. 2007. Gateway-based destination vectors for functional analyses of bacterial ORFeomes: application to the Min system in Brucella abortus. Appl Environ Microbiol 73: 1375–1379. https://doi.org/10.1128/AEM.01873-06.
52. Keseler IM, Mackie A, Peralta-Gil M, Santos-Zavaleta A, Gama-Castro S, Bonavides-Martínez C, Fulcher C, Huerta AM, Kothari A, Krummenacker M, Latendresse M, Muñiz-Rascado L, Ong Q, Paley S, Schröder I, Shearer AG, Subhraveti P, Travers M, Weerasinghe D, Weiss V, Collado-Vides J, Gunsalus RP, Paulsen I, Karp PD. 2013. EcoCyc: fusing model organism databases with systems biology. Nucleic Acids Res 41:D605–D612. https://doi.org/10.1093/nar/gks1027.
53. Ulrich K, Jakob U. 2019. The role of thiols in antioxidant systems. Free Radic Biol Med 140:14–27. https://doi.org/10.1016/j.freeradbiomed.2019.05.035.
54. Maurer LM, Yohannes E, Bondurant SS, Radmacher M, Slonczewski JL. 2005. pH regulates genes for flagellar motility, catabolism, and oxidative stress in Escherichia coli K-12. J Bacteriol 187:304–319. https://doi.org/10.1128/JB.187.1.304-319.2005.
55. Nishino K, Inazumi Y, Yamaguchi A. 2003. Global analysis of genes regulated by EvgA of the two-component regulatory system in Escherichia coli. J Bacteriol 185:2667–2672. https://doi.org/10.1128/JB.185.8.2667-2672.2003.
56. Seo SW, Gao Y, Kim D, Szubin R, Yang J, Cho BK, Palsson BO. 2017. Revealing genome-scale transcriptional regulatory landscape of OmpR highlights its expanded regulatory roles under osmotic stress in Escherichia coli K-12 MG1655. Sci Rep 7:1–10. https://doi.org/10.1038/s41598-017-02110-7.
57. Bruni GN, Kralj JM. 2020. Membrane voltage dysregulation driven by metabolic dysfunction underlies bactericidal activity of aminoglycosides. Elife 9:e58706. https://doi.org/10.7554/eLife.58706.
58. Hauryliuk V, Atkinson GC, Murakami KS, Tenson T, Gerdes K. 2015. Recent functional insights into the role of (p) ppGpp in bacterial physiology. Nat Rev Microbiol 13:298–309. https://doi.org/10.1038/nrmicro3448.
59. Te Winkel JD, Gray DA, Seistrup KH, Hamoen LW, Strahl H. 2016. Analysis of antimicrobial-triggered membrane depolarization using voltage sensitive dyes. Front Cell Dev Biol 4:29.
60. Gabel CV, Berg HC. 2003. The speed of the flagellar rotary motor of Escherichia coli varies linearly with protonmotive force. Proc Natl Acad Sci U S A 100:8748–8751. https://doi.org/10.1073/pnas.1533395100.
61. Miller JB, Koshland DE. 1977. Sensory electrophysiology of bacteria: relationship of the membrane potential to motility and chemotaxis in Bacillus subtilis. Proc Natl Acad Sci U S A 74:4752–4756. https://doi.org/10.1073/pnas.74.11.4752.
62. Quinn HJ, Cameron AD, Dorman CJ. 2014. Bacterial regulon evolution: distinct responses and roles for the identical OmpR proteins of Salmonella Typhimurium and Escherichia coli in the acid stress response. PLoS Genet 10:e1004215. https://doi.org/10.1371/journal.pgen.1004215.
63. Bakker EP, Mangerich WE. 1981. Interconversion of components of the bacterial proton motive force by electrogenic potassium transport. J Bacteriol 147:820–826. https://doi.org/10.1128/jb.147.3.820-826.1981.
64. Vanhauteghem D, Janssens GPJ, Lauwaerts A, Sys S, Boyen F, Cox E, Meyer E. 2013. Exposure to the proton scavenger glycine under alkaline conditions induces Escherichia coli viability loss. PLoS One 8:e60328. https://doi.org/10.1371/journal.pone.0060328.
65. Grossi V, Mollex D, Vinçon-Laugier A, Hakil F, Pacton M, Cravo-Laureau C. 2015. Mono- and dialkyl glycerol ether lipids in anaerobic bacteria: biosynthetic insights from the mesophilic sulfate reducer Desulfatibacillum alkenivorans PF2803T. Appl Environ Microbiol 81:3157–3168. https://doi.org/10.1128/AEM.03794-14.
66. Datsenko KA, Wanner BL. 2000. One-step inactivation of chromosomal genes in Escherichia coli K-12 using PCR products. Proc Natl Acad Sci U S A 97:6640–6645. https://doi.org/10.1073/pnas.120163297.
67. My L, Rekoske B, Lemke JJ, Viala JP, Gourse RL, Bouveret E. 2013. Transcription of the Escherichia coli fatty acid synthesis operon fabHDG is directly activated by FadR and inhibited by ppGpp. J Bacteriol 195: 3784–3795. https://doi.org/10.1128/JB.00384-13.
68. Zeghouf M, Li J, Butland G, Borkowska A, Canadien V, Richards D, Beattie B, Emili A, Greenblatt JF. 2004. Sequential peptide affinity (SPA) system for the identification of mammalian and bacterial protein complexes. J Proteome Res 3:463–468. https://doi.org/10.1021/pr034084x.
69. Thein M, Sauer G, Paramasivam N, Grin I, Linke D. 2010. Efficient subfractionation of gram-negative bacteria for proteomics studies. J Proteome Res 9:6135–6147. https://doi.org/10.1021/pr1002438.
70. Jiang L, He L, Fountoulakis M. 2004. Comparison of protein precipitation methods for sample preparation prior to proteomic analysis. J Chromatogr A 1023:317–320. https://doi.org/10.1016/j.chroma.2003.10.029.
71. Dorfer V, Pichler P, Stranzl T, Stadlmann J, Taus T, Winkler S, Mechtler K. 2014. MS Amanda, a universal identification algorithm optimized for high accuracy tandem mass spectra. J Proteome Res 13:3679–3684. https://doi.org/10.1021/pr500202e.
72. Käll L, Canterbury JD, Weston J, Noble WS, MacCoss MJ. 2007. Semi-supervised learning for peptide identification from shotgun proteomics datasets. Nat Methods 4:923–925. https://doi.org/10.1038/nmeth1113.
73. Hudson MA, Siegele DA, Lockless SW. 2020. Use of a fluorescence-based assay to measure Escherichia coli membrane potential changes in high

throughput. Antimicrob Agents Chemother 64:e00910-20. https://doi.org/10.1128/AAC.00910-20.
74. Smirnova GV, Oktyabrsky ON. 2018. Relationship between Escherichia coli growth rate and bacterial susceptibility to ciprofloxacin. FEMS Microbiology Lett 365:fnx254. https://doi.org/10.1093/femsle/fnx254.
75. Feirer N, Kim D, Xu J, Fernandez N, Waters CM, Fuqua C. 2017. The Agrobacterium tumefaciens CheY-like protein ClaR regulates biofilm formation. Microbiology (Reading) 163:1680–1691. https://doi.org/10.1099/mic.0.000558.
76. Blattner FR, Plunkett G, Bloch CA, Perna NT, Burland V, Riley M, Collado-Vides J, Glasner JD, Rode CK, Mayhew GF, Gregor J, Davis NW, Kirkpatrick HA, Goeden MA, Rose DJ, Mau B, Shao Y. 1997. The complete genome sequence of Escherichia coli K-12. Science 277:1453–1462. https://doi.org/10.1126/science.277.5331.1453.
77. Clark D. 1984. Novel antibiotic hypersensitive mutants of Escherichia coli genetic mapping and chemical characterization. FEMS Microbiology Lett 21:189–195. https://doi.org/10.1111/j.1574-6968.1984.tb00209.x.
78. Kunst F, Ogasawara N, Moszer I, Albertini AM, Alloni G, Azevedo V, Bertero MG, Bessières P, Bolotin A, Borchert S, Borriss R, Boursier L, Brans A, Braun M, Brignell SC, Bron S, Brouillet S, Bruschi CV, Caldwell B, Capuano V, Carter NM, Choi S-K, Codani J-J, Connerton IF, Cummings NJ, Daniel RA, Denizot F, Devine KM, Düsterhöft A, Ehrlich SD, Emmerson PT, Entian KD, Errington J, Fabret C, Ferrari E, Foulger D, Fritz C, Fujita M, Fujita Y, Fuma S, Galizzi A, Galleron N, Ghim S-Y, Glaser P, Goffeau A, Golightly EJ, Grandi G, Guiseppi G, Guy BJ, Haga K, et al. 1997. The complete genome sequence of the Gram-positive bacterium Bacillus subtilis. Nature 390:249–256. https://doi.org/10.1038/36786.
79. Amann E, Ochs B, Abel KJ. 1988. Tightly regulated tac promoter vectors useful for the expression of unfused and fused proteins in Escherichia coli. Gene 69:301–315. https://doi.org/10.1016/0378-1119(88)90440-4.
80. Guzman LM, Belin D, Carson MJ, Beckwith J. 1995. Tight regulation, modulation, and high-level expression by vectors containing the arabinose PBAD promoter. J Bacteriol 177:4121–4130.